KTH Engineering Sciences

Pulsed Yb:KYW laser and UV generation

Staffan Tjörnhammar

Master of Science Thesis

Laser Physics
Department of Applied Physics
School of Engineering Science
KTH

Stockholm, Sweden 2010

TRITA-FYS: 2010:29
ISSN: 0280-316X
ISRN: KTH/FYS/- -10:29- -SE

Abstract
In this master thesis project, a pulsed UV laser was designed and constructed. Also, the effects of absorption in a volume Bragg grating were investigated.

The laser was diode pumped and constructed with Yb:KYW as gain medium. The lasing was at a wavelength of 1029.2 nm with a spectral bandwidth of 0.23 nm, locked by a volume Bragg grating that was used as input coupler for spectral control. Passive Q-switching was used to generate pulses by placing a Cr:YAG saturable absorber inside the cavity. The laser generated radiation with a maximum peak power of 3.8 kW at an average power of 0.35 W, a repetition rate of 4 kHz and a pulse width of 16 ns. The maximum average power was 1.3 W with a peak power of 2 kW at a repetition rate of 20 kHz and with a pulse width of 20 ns. Through extra-cavity second harmonic generation using an LBO crystal, green light at a wavelength of 514.7 nm was generated. The maximum average power was 130 mW with an optical conversion efficiency from the fundamental of around 10 %. Then, the second harmonic and the fundamental wave were mixed to generate UV light, at a wavelength of about 343 nm, by using a second LBO crystal. The maximum average power of UV was about 23 mW with an optical efficiency, with respect to the green, of approximately 20 %. One limitation of the laser was that the Cr:YAG was bleached not only by the circulating laser field, but also by remaining pump light. This resulted in decreasing peak power with increasing pump power, thus limiting the nonlinear conversion efficiencies. Thermal fracture of the Cr:YAG was a limiting factor for the intra-cavity average power, while burning of the coating on the Yb:KYW crystal limited the maximum peak power.

The effects on a laser when using too high power for the level of absorption in a volume Bragg grating were also investigated. The effects of both resonant and non-resonant beams were investigated. Since the intensity of a resonant beam decreases approximately exponentially in a volume Bragg grating, due to absorption, an uneven temperature distribution along the propagation axis is formed. This results in different thermal expansion and hence, results in a longitudinal chirp of the grating. The chirp caused a decrease in both reflectivity and spectral selectivity. The reflectivity of the particular grating used in these experiments decreased from 99.4 % to 93 %. In addition, it was experimentally shown that if a volume Bragg grating absorbs a non-negligible amount of a non-resonant beam, the thermal load will deform the volume Bragg grating. Therefore, it is not suitable to use such a grating the as input coupler of a laser cavity.

Sammanfattning
I detta examensarbete utformades och konstruerades en pulsad UV-laser. Dessutom undersöktes effekterna av absorption i ett volymbraggitter.

Som laserkristall användes Yb:KYW vilken pumpades med en diodlaser. Lasring skedde vid 1029,2 nm med en bandbredd av 0,23 nm genom att ett volymbraggitter användes som inkopplingsspegel för att kontrollera spectrumet. Pulser generades genom passiv Q-switching med en Cr:YAG som mättnadsbar absorbator inne i kaviteten. Den maximala toppeffekten var 3,8 kW vid 0.35 W medeleffekt, 4 kHz repetitionsfrekvens och en pulsbredd på 16 ns. Den maximala medeleffekten var 1.3 W med en toppeffekt på 3,8 kW, 20 kHz repetitionsfrekvens och en pulsbredd på 20 ns. Genom frekvensdubbling i en LBO kristall genererades grönt ljus vid våglängden 514,7 nm. Den maximala medeleffekten var 130 mW med en optisk verkningsgrad från den fundamentala våglängden på 10 %. Sedan blandades det infraröda och det gröna ljuset i en andra LBO kristall för att generera UV-ljus, vid en våglängd om 343 nm. Den högsta medeleffekten av UV var cirka 23 mW med en optisk verkningsgrad, med avseende på det gröna ljuset, på ungefär 20%. En begränsning av laser var att Cr:YAG kristallen blektes inte enbart av lasern utan även av pumpen. Detta resulterade i fallande toppeffekt med ökande pumpeffekt, vilket begränsade effektiviteten i den ickelinjära konverteringen. Termisk fraktur på Cr:YAG kristallen var en begränsande faktor för cirkulerande medeleffekten i kaviteten, medan brännskador på Yb-kristallens antireflexbehandling begränsade toppeffekten.

Effekterna i en laser vid användning av en alltför hög effekt i förhållande till nivån av absorption i ett volymbraggitter studerades också. Effekterna av både resonanta och ickeresonanta strålar undersöktes. Eftersom intensiteten av en resonant ståle minskar ungefär exponentiellt i ett volymbraggitter kommer temperaturen, på grund av absorption, fördelas ojämnt i propageringsriktningen. Detta resulterar i olika termiska expansion med en längsgående varierad gitterperiod som följd. Detta orsakar en minskning utav både reflektiviteten och den spektrala selektiviteten. Reflektiviteten i gittret som användes i dessa experiment minskade från 99,4 % till 93 %. Dessutom visades det experimentellt att om ett volymbraggitter absorberar en icke försumbar del av en ickeresonant stråle kommer värmebelastning att deformera volymenbraggittret. Därför är det inte lämpligt att använda ett sådant gitter som inkopplingsspegel i en laser.

Acknowledgements
I would like to thank my supervisor Dr. Björn Jacobsson. He has contributed with a priceless amount of knowledge, skill and feedback.

I also thank my other supervisor Kai Seger for all his help and support.

I am grateful to Prof. Fredrik Laurell and Prof. Valdas Pasiskevicius for allowing me to do this project in their group and for all their knowledge and support.

I would like to express my gratitude to Kai Seger and Niels Meiser for letting me use their measurement in this thesis.

To Hoon Jang, who has allowed me to use his software and given me feedback on this thesis I would like to say thank you, you are a good friend.

I would like to thank assoc. Prof. emeritus Jens A. Tellefsen, Jr. for all his help and knowledge.

I would like to express my gratitude to all the members of the Laser physics research group. They never hesitate to share their knowledge or to give a helping hand. I have enjoyed working with you.

Last but not least, I thank my wife Janeth Tjörnhammar for her understanding and for being patient with me. Without her covering for me at home none of this would have been possible.

Contents

1 Introduction 1

1.1 Background 1

1.2 The objective of the work 1

1.3 The outline of the thesis 1

2 Laser principles 3

2.1 The knife-edge technique 6

2.2 Volume Bragg grating 8

2.3 Solid-state lasers 8

2.4 Q-switching 11

2.5 Nonlinear optics 12

3 The pump laser 14

4 Ordinary Yb:KYW lasers 16

4.1 Linear cavity laser with a 2 mm long Yb:KYW crystal 16

4.2 Optimization of the output power of the laser with a 2 mm long Yb:KYW crystal 18

4.3 Linear cavity laser with a 3 mm long Yb:KYW 21

4.4 Folded cavity laser with a 3 mm long Yb:KYW 22

5 Lasers with the long VBG – thermal effects 25

5.1 Linear cavity laser with the VBG as input coupler 25

5.2 Folded cavity – thermal effects for resonant beams 30

5.3 Discussion 33

6 Lasers with the short VBG 36

6.1 Linear cavity cw laser 36

6.2 Pulsed laser 39

6.3 Second harmonic generation to green 44

6.4 Sum frequency generation to UV 46

6.5 Damage to components 50

6.6 Discussion 51

7 References 53

1 Introduction

1.1 Background

Many materials absorb electromagnetic radiation in the ultraviolet (UV) spectral range. This together with the possibility of achieving a small diffraction-limited spot size makes UV lasers a good tool for material processing, e.g. micromachining and microlithography. Other common applications are ultraviolet spectroscopy and nonlinear spectroscopy. There are two common types of UV lasers. The first one is gas lasers, such as Argon and Nitrogen lasers with laser lines at 351 nm and 337 nm, respectively. Gas lasers have the disadvantage of low power efficiency and limited life time. The second one is diode-pumped solid-state lasers, lasing around 1 μm, used together with multiple nonlinear processes to generate a laser beam in the ultraviolet region.

Ytterbium doped monoclinic double tungstates, e.g. Yb:KYW and Yb:KGW, make a good choice when choosing the gain medium for a diode-pumped solid-state laser. Ytterbium has a broad emission spectrum which allows, together with some measure for spectral control, a wide range of wavelength to choose from. It is possible to pump Ytterbium at 980 nm, a wavelength where there are good laser diodes available, since Erbium doped optical fibers, used in telecommunications, have been pumped at this wavelength for many years now. To achieve good nonlinear conversion there are three criteria of the laser beam that needs to be fulfilled. Firstly, the light needs to be linearly polarized; this is automatically achieved when using double tungstates as host material. Secondly, since the nonlinear conversion is wavelength dependent, a narrow spectrum free from fluctuations is required. In this work this was achieved by using a volume Bragg grating as a laser cavity component. Volume Bragg gratings have a narrow reflectivity bandwidth, e. g. 0.4 nm, and are transparent for other wavelengths. Thirdly, high electric field strength is required, since nonlinear conversion have a nonlinear dependence of the electric field of the fundamental wave. This can be achieved by using pulses. An easy way to generate pulses is to use passive Q-switching by placing a saturable absorber inside the cavity.

1.2 The objective of the work

The aim of this master thesis project was to be design and construct a pulsed UV-laser. As laser gain medium Yb:KYW crystals were used, pumped at 980 nm for lasing at 1030 nm. A volume Bragg grating (VBG) was used in the design of the laser to lock the wavelength. For the passive Q-switching a Cr:YAG crystal was placed inside the laser cavity. To create UV-light, the fundamental frequency was externally doubled to 515 nm by using a nonlinear crystal (LBO). The fundamental and the second harmonic was than mixed to generate the third harmonic (343 nm) through sum frequency generation, by using a second nonlinear crystal (LBO).

1.3 The outline of the thesis

This thesis is organized as follows:

In chapter 2 some basic theory relevant to the work is briefly described as an introduction to the subject.

In chapter 3 the characterization of the pump laser is presented.

In chapter 4, lasers constructed with a dielectric mirror as input coupler is described. These lasers were built as a first step towards constructing a cavity with a volume Bragg grating used for spectral control.

In chapter 5, experiments are described that show the effects when the absorption of the volume Bragg grating is too high for the powers used in a laser. In the last section of the chapter, the results from the experiments are discussed and suggestions for future work on the subject are given.

In chapter 6, laser experiments with a volume Bragg grating used for spectral control, the generation of pulses through Q-switching, second harmonic generation and sum frequency generation are described. In the last section of the chapter the results from the experiments are discussed and suggestions for future work on the subject are given.

2 Laser principles

In this chapter some brief theory relevant to the work, the method used to measure beam quality and some material properties are described.

Basic laser theory

Introduction

The principal of a laser is that it consists of a resonance cavity and an amplifying medium, also known as *gain-medium*. The resonance cavity is often constructed with a high-reflecting mirror and a partly reflecting mirror, also known as the output coupler (OC), see Fig. 2.1. The light transmitted through the OC is known as the laser beam. Since most OCs only transmits a small portion (e.g. 10 %) of the incident light, the power circulating inside the cavity is much higher (e.g. 10 times) than the power of the laser beam.

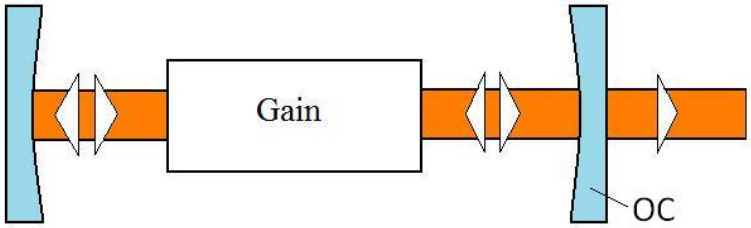

Figure 2.1: *Schematic drawing of a basic laser cavity.*

It is when the light passes through the gain-medium that it is amplified by a process called *stimulated emission*. Stimulated emission is when an electron in an exited state is stimulated by an incoming photon to fall down to a lower energy level by emitting a photon, see Fig 2.2. The emitted photon will have the same wavelength and phase as the incoming one. Excited atoms emit photons in random directions, this is called *spontaneous emission*. Spontaneous emission is what starts the laser.

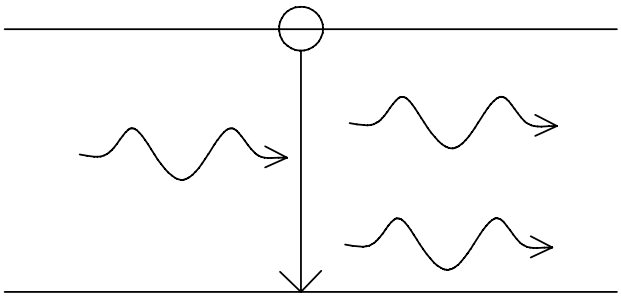

Figure 2.2: *Schematic drawing of stimulated emission.*

One condition for the gain-medium to work as an amplifier is that its energy levels are populated in such a way that an incoming photon has higher probability to generate a new photon than being absorbed. If that is the case the system has *population inversion*. However, at thermal

equilibrium the lower energy level is more populated than the higher energy level. It is therefore necessary to add energy to the gain-medium for laser action to occur, this is known as *pumping*. If the laser is supposed to continuously emit light (*continuously wave* or *cw*) continuous pumping is necessary.

The threshold is the lowest pump power for which the gain medium is pumped to the level that the roundtrip gain equals to the cavity losses.

Longitudinal Modes

The wavelength of light that can find resonance in a cavity needs to fulfill the condition that half the wavelength (λ) multiplied with an integer number (m) equals to the optical pass length (L) of the cavity as:

$$m\frac{\lambda}{2} = L \tag{2.1}$$

In most cases the value of m is large since the wavelength is much shorter than the optical pass length (e.g. $m = 10^5$ for $\lambda = 1\mu m$ and $L = 50$ mm). It follows from Eq. 2.1 that the frequency separation ($\Delta\nu$) between two adjacent longitudinal modes equals to the speed of light in vacuum (c) divided by twice the optical pass length as:

$$\frac{c}{2L} = \Delta\nu \tag{2.2}$$

As one can see, the mode separation is dependent on the length of the cavity.

Transverse Electromagnetic Modes

There are several different ways that the light circulating in the cavity can resonate depending on the spatial boundary conditions of the cavity. These different resonance ways are called transverse electromagnetic modes. Each mode has its own intensity distribution described by [1]:

$$I_{m,n}(x,y) = I_0\left[H_m\left(\frac{\sqrt{2}x}{\omega}\right)H_n\left(\frac{\sqrt{2}y}{\omega}\right)e^{-(x^2+y^2)/\omega^2}\right]^2 \tag{2.3}$$

Here $H_{m/n}$ is the Hermite polynomial of order m/n, I_0 is the maximum intensity, ω is the beam radius and x and y are orthogonal transverse directions. It is common to denote these modes TEM_{mn}, and the mode when $n = m = 0$ is known as the fundamental mode and all other combinations are higher order modes. For most cases, the fundamental mode is the one that is desired when designing a laser. In Fig. 2.3 the intensity distributions for some transverse modes are shown.

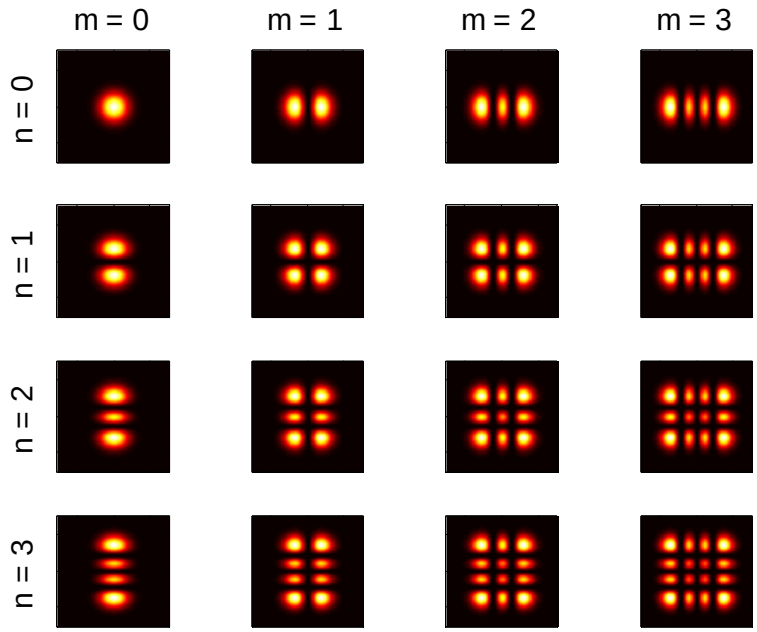

Figure 2.3: *Intensity distributions for some transverse electromagnetic modes.*

Gaussian beam

A laser operating in the fundamental transverse mode has a beam with a Gaussian intensity distribution in the transverse direction, known as a Gaussian beam. Even if the Gaussian distribution stretches out to infinity it is convenient to talk about beam size. One commonly used definition of the beam radius is the distance where the intensity has dropped to $1/e^2$ of the maximum intensity. Gaussian beams have a smallest beam radius, ω_0, known as beam waist, and the radius at any point, ω, depends of the size of the waist as [1]:

$$\omega(z) = \omega_0 \left[1 + \left(\frac{\lambda z}{\pi {\omega_0}^2}\right)^2\right]^{1/2} \tag{2.4}$$

Here the z-axis is the beam propagation direction, the coordinate of the beam waist is $z = 0$ and λ is the wavelength.

The depth of focus, when focusing a Gaussian beam, is known as the Rayleigh range, z_R. It is the distance where the radius has increased by $\sqrt{2}$ relative to the beam waist, and it follows from Eq. 2.4 that it can be described by:

$$z_R = \frac{\pi {\omega_0}^2}{\lambda} \tag{2.5}$$

For distances much larger than the Rayleigh range, the divergence angle is given by:

$$\theta = \frac{2\lambda}{\pi \omega_0} \tag{2.6}$$

Here θ is the full angle of the diverging Gaussian beam to the point when the intensity has dropped to $1/e^2$ of the maximum value.

A Gaussian beam is often referred to as a diffraction limited beam since it can be focused down to the smallest diffraction limited spot size.

Beam quality factor

Most laser beams are not pure Gaussian beams since real lasers often operate in multi transverse modes, and the formulas describing the Gaussian beam are for that reason not applicable. However, real beams can be defined via multiples of the ideal Gaussian beam. For that reason the factor M has been introduced. It makes it possible to describe the divergence angle, Θ, and the beam waist, W_0, of the real beam as follows:

$$\Theta = M\theta \tag{2.7}$$

$$W_0 = M\omega_0 \tag{2.8}$$

This allows Eq. 2.4. to be modified to fit a real laser beam with, $W(z)$ as the $1/e^2$ beam radius at any point on the z-axis and W_0 as the beam waist for a real beam.

$$W(z) = W_0\left[1 + \left(M^2\frac{\lambda z}{\pi {W_0}^2}\right)^2\right]^{1/2} \tag{2.9}$$

As seen it is not M but M^2 that separates Eq. 2.9 from Eq. 2.4 and it is M^2 that is known as the *beam quality factor* or *beam propagation factor*. A laser beam is said to be M^2 times diffraction limited. From Eq. 2.9 it follows that the Rayleigh range of a real laser beam will be described by:

$$z_R = \frac{\pi {W_0}^2}{M^2\lambda} \tag{2.10}$$

2.1 The knife-edge technique

The knife-edge technique is a method by simple means to determine the M^2 factor of a laser beam. The equipment needed is a power meter, a lens and a razor-blade placed on a translation stage with micrometer precision. The beam is focused by the lens and the radius is measured for several points along the z-axis (beam propagation direction) starting at some distance before the focus and stopping at some distance, much larger than Rayleigh range, after the focus. The beam waist, W_0, and the M^2 factor are obtained by fitting Eq. 2.9 to the measured data. The beam radius is measured by cutting the beam perpendicular to the propagation direction with the razor-blade, shadowing out a part of the beam. The radius is the distance the razor-blade has moved between the two points where 84 % and 16 % of the total beam power is passing the razor-blade, as schematically depicted in Fig. 2.4.

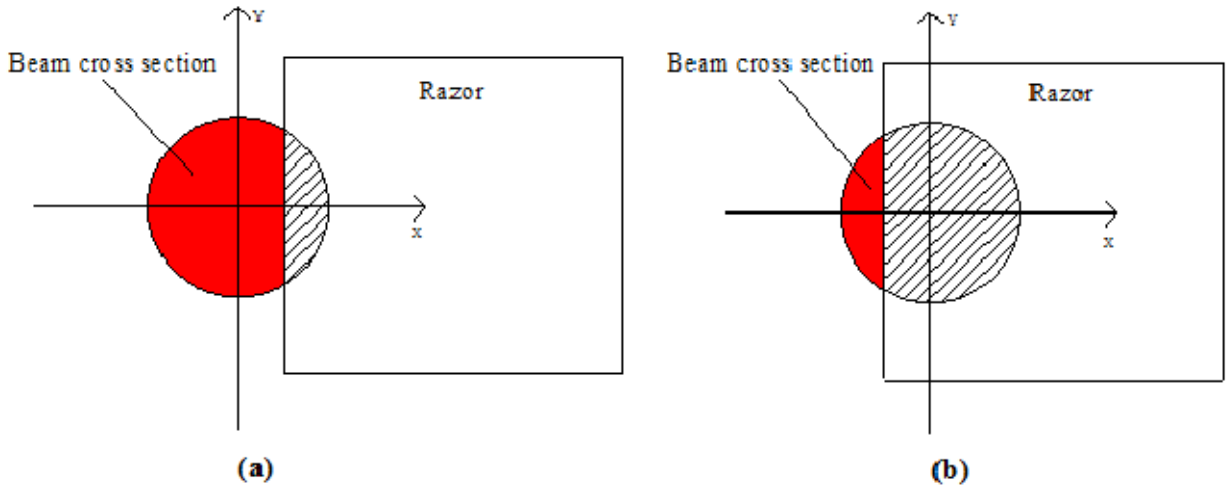

Figure 2.4: *In (a) the razor-blade is blocking 16 % of the total power, in (b) the razor-blade is blocking 84 % of the total power.*

The motivation for using these points for measurement is that the laser beam is assumed to be Gaussian or at least close to Gaussian. This means that the total power (P_{tot}) is obtained by integrating the Gaussian distribution (Eq. 2.1. with $m = n = 0$) from minus infinity to infinity in both Cartesian directions with the origin in the center of the beam:

$$P_{tot} = I_0 \int_{-\infty}^{\infty} e^{-2\frac{x^2}{\omega^2}} dx \int_{-\infty}^{\infty} e^{-2\frac{y^2}{\omega^2}} dy = I_0 \frac{1}{2} \omega^2 \pi \tag{2.11}$$

When the razor-blade blocks a part of the beam, the blade moves along the x-axis with the edge at some arbitrary coordinate X. The power passing the beam, $P(X)$, is given by:

$$P(X) = I_0 \int_{-\infty}^{X} e^{-2\frac{x^2}{\omega^2}} dx \int_{-\infty}^{\infty} e^{-2\frac{y^2}{\omega^2}} dy = I_0 \frac{1}{4} \omega^2 \pi \left(1 + \mathrm{erf}\left(\frac{\sqrt{2}X}{\omega}\right)\right) \tag{2.12}$$

Here the error function, erf(z), is defined as:

$$\mathrm{erf}(z) \equiv \frac{2}{\sqrt{\pi}} \int_{0}^{z} e^{-t^2} dt \tag{2.13}$$

The ratio of the blocked beam power to total beam power is approximately 84 % if $X = \omega/2$ and 16 % if $X = -\omega/2$, Eq. 2.14.

$$\frac{P(X)}{P_{tot}} = \begin{cases} \frac{1}{2}\left(1 + \mathrm{erf}\left(\frac{\sqrt{2}}{2}\right)\right) \approx 0.84 & if\ X = \frac{\omega}{2} \\ \frac{1}{2}\left(1 - \mathrm{erf}\left(\frac{\sqrt{2}}{2}\right)\right) \approx 0.16 & if\ X = -\frac{\omega}{2} \end{cases} \tag{2.14}$$

2.2 Volume Bragg grating

A volume Bragg grating or VBG is a bulk piece of glass with periodic variations in refractive index. All VBGs used in this thesis had sinusoidal variations of refractive index. This makes them transparent for all wavelengths except those that meet the Bragg condition:

$$\lambda = 2n\Lambda \cos\theta \tag{2.15}$$

Here Λ is the grating period, λ is the wavelength in vacuum of light, n is the refractive index and θ is the angle between the propagation direction of the light and the normal of the grating.

The reflectivity of a VBG is strongly wavelength dependent and the reflection bandwidth is usually very narrow (e.g. 0.4 nm). This property of VBGs makes them suitable as optical components when one wants to lock the spectrum of a laser.

2.3 Solid-state lasers

Solid-state lasers are lasers that have a gain medium consisting of a transparent dielectric host material doped with the active medium, such as lanthanide or transitional-metal ions. It is common to optically pump solid-state lasers by using a flash lamp or a laser diode (semiconductor laser). Pumping by a laser diode has the advantage of a narrower spectrum than a flash lamp. This means that by matching the wavelength from the diode laser to the absorption spectrum of the gain medium it is possible to achieve higher power efficiency.

Thermal lens

Thermal lensing can appear in a laser crystal when it is heated. It can be due to a transverse temperature gradient leading to a transverse gradient of the index of refraction (the thermo-optic effect). Also thermally induced mechanical stress leading to changes in the index of refraction (photo-elastic effect) and bulging of the end faces have lensing effects.

A thermal lens can reshape the mode inside the cavity and lead to lower stability and mismatch between the mode and the pump.

Yb:KYW

Ytterbium doped potassium yttrium tungstate or Yb:KYW is commonly used as a gain medium in diode-pumped solid-state lasers. As shown in Fig. 2.5, Yb:KYW has a large absorption cross-section at 980 nm. This is a wavelength where there are high power laser diodes available, since Erbium doped fiber, used in telecommunications, have been pumped at this wavelength for many years. As one can see in Fig. 2.6, the emission cross-section has a broad spectrum which, together with some measure for spectral control, allows engineering of lasers at a wide range of wavelengths. Also, the broad emission spectrum make Yb:KYW to a suitable gain medium when designing a tunable laser [2]. The energy levels involved when lasing in Yb^{3+} are the $^2F_{7/2}$ and $^2F_{5/2}$ levels with their respective Stark sublevels [3]. This means that there is no parasitic loss due to upconversion processes in other levels, like in Neodymium. As shown schematically in

Fig. 2.7, the laser was operated as a three level system, pumped directly into the upper laser level with a wavelength around 981 nm and lasing at a wavelength around 1030 nm. This gives a quantum defect just below 5 %. Low quantum defect is important to limit the thermal effects (e.g. thermal lensing) in the system. The crystal structure of KYW is biaxial, with three orthogonal dielectric axes named N_g, N_m, and N_p, where $N_g > N_m > N_p$ referring to the refractive index. The largest cross-sections are in the N_m polarization axis. A crystal cut for beam propagation along one of the two other axes will generate light linearly polarized in the N_m direction. This is of great advantage when the laser is to be used for nonlinear conversion.

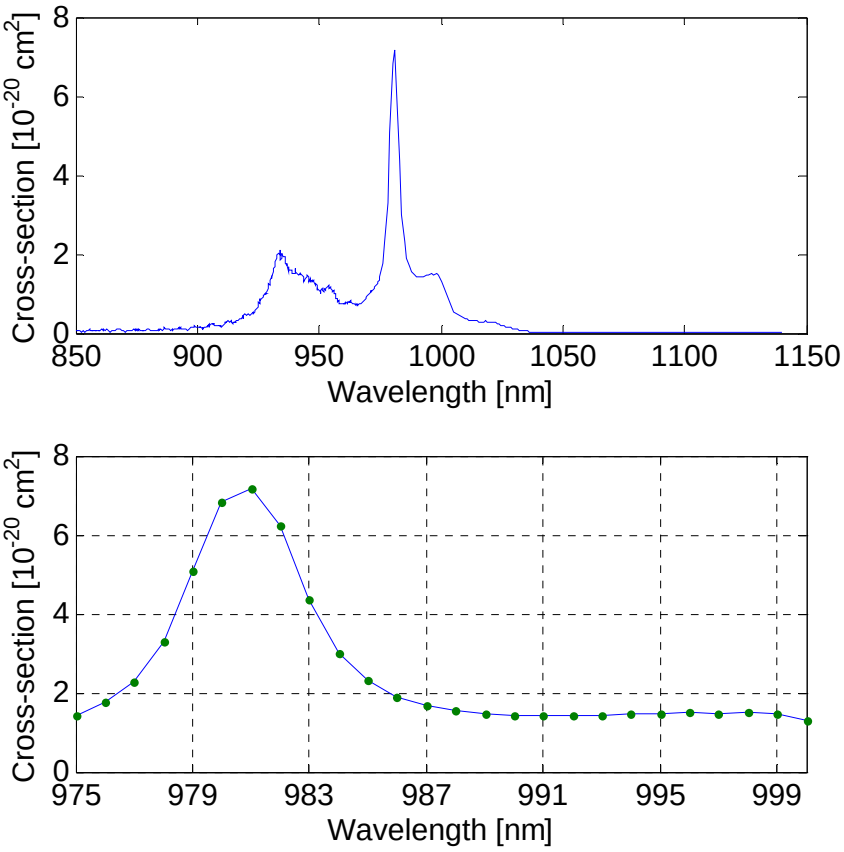

Figure 2.5: *Absorption cross-section for Yb:KYW in N_m polarization* [4].

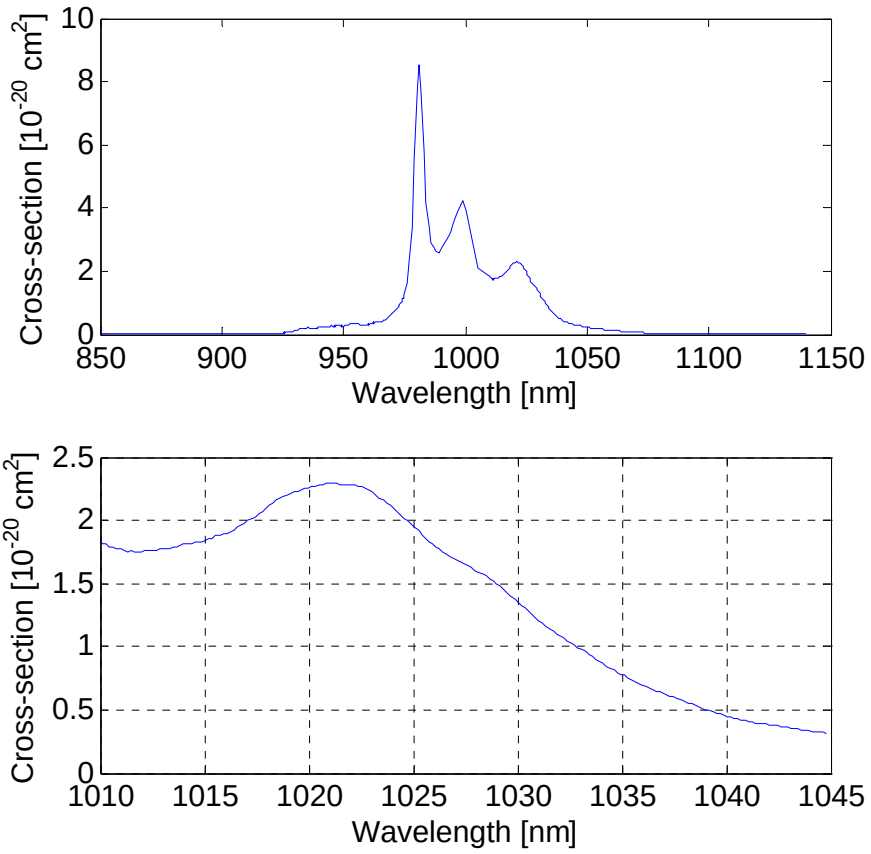

Figure 2.6: *Emission cross-section for Yb:KYW in N_m polarization* [4].

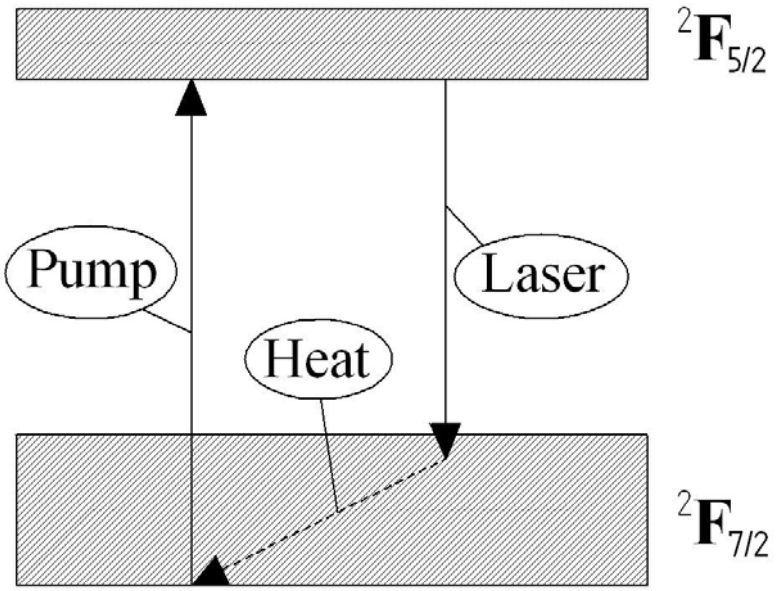

Figure 2.7: *Energy level diagram of a Yb:KYW laser.*

2.4 Q-switching

Q-switching is a technique used to create intense laser pulses. The quality factor or Q-factor is a measure of the quality of the resonant cavity; a high Q value indicates low losses.

To generate pulses, a "shutter" is introduced in to the laser cavity. When the shutter is closed the Q value is low and laser action is suppressed. This allows the gain medium to be pumped to a higher level of population inversion compared to being operated in cw. Then the shutter is opened and the Q value is rapidly switched to a high one, and the stored energy is released in a pulse [5].

Q-switched lasers can be either actively or passively Q-switched. In active Q-switching the losses comes from a controlled element (e.g. an electro-optic modulator), while in passive Q-switching, a saturable absorber is placed inside the cavity. A saturable absorber is a substance with an excited state life time long enough for it to saturate. When the substance is saturated it becomes bleached and the laser pulse begins to build up. To achieve a large pulse it is important that the saturable absorber saturates before the gain saturates [6].

Cr^{4+}:YAG as saturable absorber

A commonly used saturable absorber is a YAG (yttrium aluminum garnet, $Y_3Al_5O_{12}$) crystal doped with chromium (Cr^{4+}) ions, often denoted Cr:YAG. It has a high absorption cross-section in the 0.9 to 1.2 μm region ($5 \cdot 10^{-18}$ cm^{-2} at 1.06 μm [7]). Also, it has a fairly high damage threshold, good thermal conductivity and is chemically stable. It can be manufactured very thin, so it is possible to use it in side small cavities. These properties make it an attractive choice when designing Q-switched solid-state lasers.

The energy levels involved can be described as a four-level system (Fig. 2.8) [8]. The transition from E1 to E3 is the desired absorption transition called ground state absorption (GSA) with a corresponding cross section σ_{gsa}. From E3 the electron rapidly decays to E2 and the lifetime for the spontaneous decay from E2 to E1 is in the order of microseconds, see [9] and references therein. The long lifetime in E2 allows the Cr^{4+}:YAG to bleach and work as a saturable absorber. However, absorption also occurs in the transition from E2 to E4 with a corresponding cross section σ_{esa}, known as excited state absorption (ESA), and the lifetime for decay from E4 to E2 is in the order of picoseconds, see [9] and references therein. The ESA normally does not saturate and it is experienced as a parasitic loss in the cavity. Over the last ten years there have been several good results reported on using Cr^{4+}:YAG as saturable absorber together with ytterbium doped double tungstates [10] [11] [12] [13].

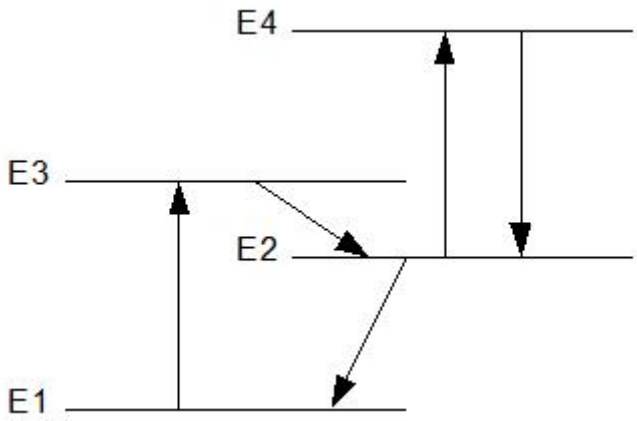

Figure 2.8: *Energy diagram of Cr:YAG.*

2.5 Nonlinear optics

The word non-linear in non-linear optics refers to how the induced polarization in a dielectric medium depends on the applied electric field. The induced polarization, *P*, can be described in a generalized form by a power series in the strength of the electric field, *E*, [14]:

$$P = \varepsilon_0\left[\chi^{(1)}E + \chi^{(2)}E^2 + \chi^{(3)}E^3 + \ldots\right] \tag{2.16}$$

Here ε_0 is the vacuum permittivity and $\chi^{(n)}$ is the *n*-th order optical susceptibility tensor. The first term on the right hand side is known as the linear polarization, P^L, and the following terms as the nonlinear polarization, P^{NL}. For most materials the non-linear part is so weak it can be neglected and the polarization is described by P^L. All nonlinear processes in this thesis were of the second order. In the cases where the conditions for Kleinman symmetry holds the susceptibility tensor containing 27 elements is usually replaced with the *d* tensor containing 18 elements. According to the definition $2d = \chi^{(2)}$. For given directions of the polarization and the propagation through a material, *d* has an effective value known as the effective nonlinear coefficient, denoted d_{eff} [14]. The non-linear polarization, P^{NL}, can now be described by:

$$P^{NL} = 2\varepsilon_0 d_{eff} E^2 \tag{2.17}$$

If the applied electric field is of one frequency, as in the case of second harmonic generation (SHG), it can be described by:

$$E = A(\omega)e^{-i(\omega t - k_\omega z)} + c.c. \tag{2.18}$$

Here $A(\omega)$ is the amplitude of the field, ω is the angular frequency, *t* is time, *z* is the direction of the beam propagation and k_ω is the wave vector for the frequency ω:

$$k_\omega = \frac{n(\omega)\omega}{c} \tag{2.19}$$

Here $n(\omega)$ is the refractive index at ω and *c* is the speed of light in vacuum.

The electric field of the desired second harmonic wave can be described by:

$$E = A(2\omega)e^{-i(2\omega t - k_{2\omega} z)} + c.c. \tag{2.20}$$

The generated wave will, however, according to Eq. 2.17 be described by:

$$E = A(2\omega)e^{-i(2\omega t - 2k_\omega z)} + c.c. \quad (2.21)$$

The demand for Eq. 2.21 to be equal to Eq. 2.20 is that k_ω equals to $k_{2\omega}$. This is, however, often not the case since the refractive index is frequency dependent. This leads to a phase mismatch (Δk) given by:

$$\Delta k = k_{2\omega} - k_\omega \quad (2.22)$$

The consequence of the phase mismatch is that energy will be transferred back and forth between the fundamental wave and the second harmonic wave as the beams propagates through the nonlinear medium. For the nonlinear conversion to be effective, the phases needs to be matched ($\Delta k = 0$), something that can be achieved with birefringent phase matching.

Birefringent phase matching

Birefringent phase matching (BPM) uses the natural birefringence of some crystals to solve the phase mismatch problem. When linearly polarized light propagates through the crystal, the refractive index will depend on the direction of the polarization. So for certain directions in the crystal, waves of different frequency and polarization can experience the same refractive index. A second order nonlinear process involves three interacting waves, ω_1, ω_2 and ω_3 where $\omega_3 = \omega_2 + \omega_1$ ($\omega_1 = \omega_2$ for the case of SHG). If ω_1 and ω_2 has the same direction of polarization the phase matching is of type I, in the case where they are perpendicular to each other the phase matching is of type II. One disadvantage of using BPM is that the propagation direction through the crystal where the phase matching condition is fulfilled does not necessary have a large nonlinear coefficient. Also, the interacting waves can experience a special walk-off known as the Poynting-vector walk-off.

Lithium triborate or LBO is a nonlinear crystal that is commonly used for birefringent phase matching. It is a biaxial crystal with orthorhombic structure and a wide transparency range (160 nm to 2.6 μm [15]). LBO was chosen because it has a large acceptance angle and a low Poynting-vector walk-off, which allowed a crystal length of 10 mm. Also, LBO has a high damage threshold.

3 The pump laser

In this chapter, the characterization of the pump laser that was used in the experiments is presented. Experiments were conducted to measure the output power, the spectrum and the beam quality factor.

The pump laser was a fiber-coupled multiple-emitter diode laser. The fiber had a core diameter of 75 μm and numerical aperture of 0.22. The beam from the fiber was collimated by a lens with 11 mm focal length. The diodes emitted linearly polarized light, but the polarization was not conserved through the fiber. The difference in power for two perpendicular polarization directions was measured to be at maximum 5 %.

First, the output power from the pump laser was measured at different drive currents as shown in Fig. 3.1. The temperature was set to 18 ^{o}C with no deviation larger than 0.1 ^{o}C. The threshold was about 1.5 A drive current and the maximum output power was around 22 W at 44 A of current.

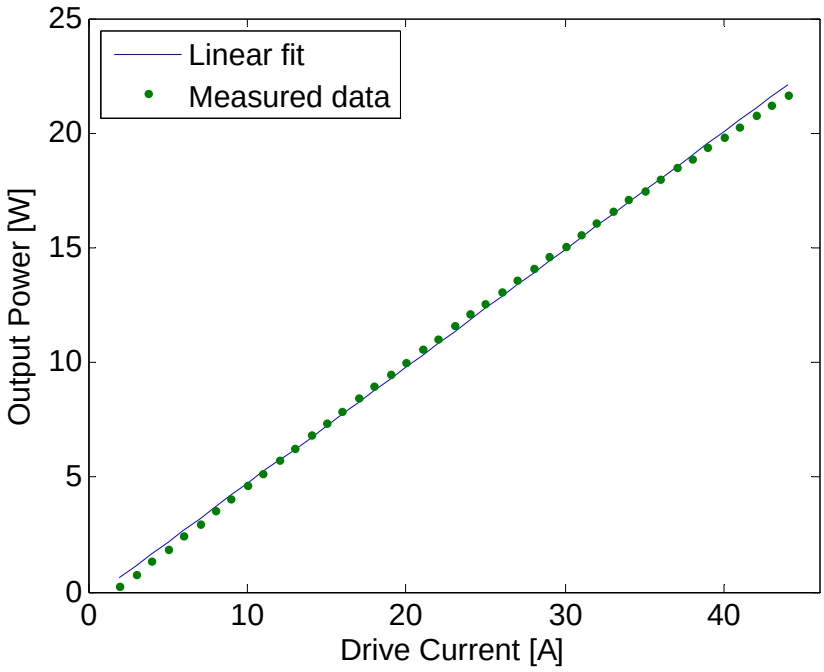

Figure 3.1: *Output power from the pump laser vs. drive current.*

Second, an optical spectrum analyzer (Hewlett-Packard 86140A) with a resolution bandwidth of 0.07 nm was used to analyze the spectrum (Fig. 3.2). The beam was attenuated and focused by a lens with focal length of 50 mm into the spectrum analyzer via a multi mode fiber. This was to ensure that the spectrum of all emitters was collected. On the contrary, when the beam was not focused, it was observed that the spectrum was different for different parts of the beam, since different emitters were measured.

The temperature of the diode holder was set to be 22.5 ^{o}C and 25.0 ^{o}C. For each set, the drive current was varied from 34 A to 44 A in steps of 0.5 A.

The result is shown in Fig. 3.2 and shows that the wavelength of the laser is tunable by changing the temperature. The temperature needs to be optimized to increase the absorption in the Yb crystal in the experiment. Even though the temperature of diode holder was stabilized using a temperature controller, the wavelength was shifted towards longer wavelengths with increasing power. When the drive current is increased it increases the temperature in the active layer and the energy band gap decreases. Thus, optimal temperature can change when the pumping power is changed.

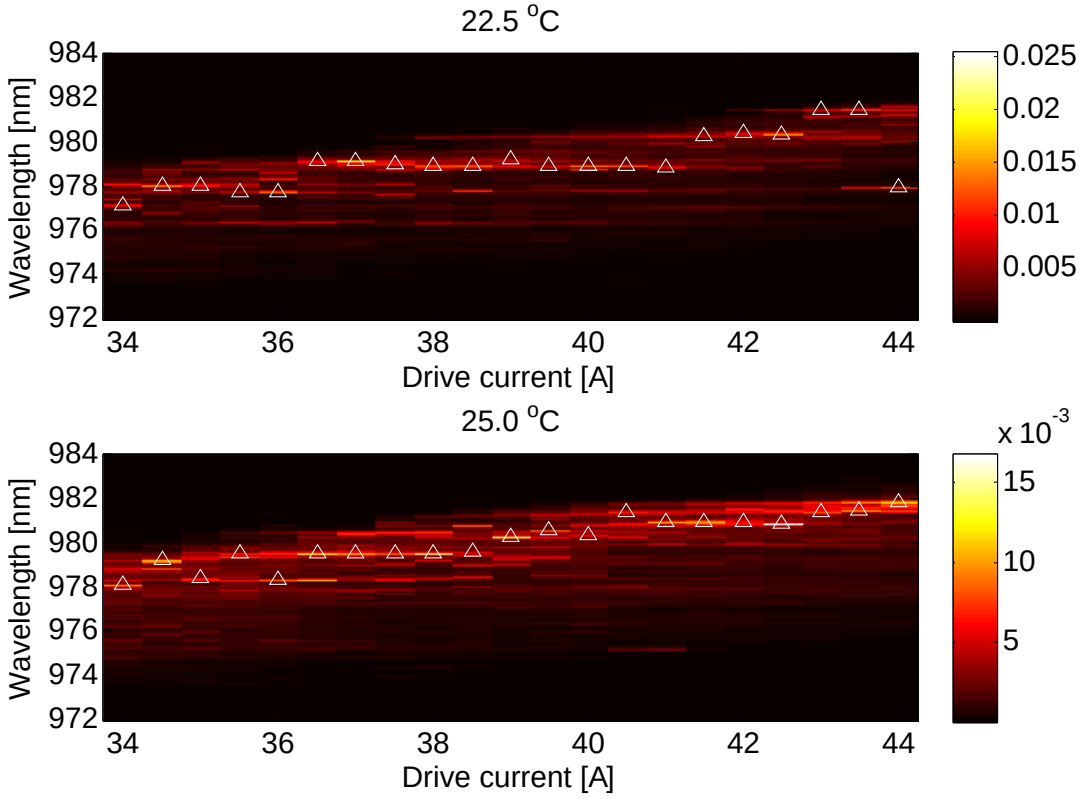

Figure 3.2: *Topographic picture of the relative powers at different wavelengths for the different drive currents put in to the pump laser. The triangles mark the peaks.*

The beam quality factor, M^2, was measured to be about 33 using the knife-edge technique as described in Sec. 2.1. This method, however, requires that the beam should be fairly close to Gaussian. The model becomes less valid for larger M^2 factors due to the reason described in Sec. 2.1.5. This result can, however, still be useful for simulations when the laser system is designed, although one should keep in mind that actual experiments may behave differently from the simulations.

4 Ordinary Yb:KYW lasers

In this chapter, a number of Yb:KYW lasers built with an ordinary dielectric mirror as input coupler are described. These lasers were built as a first step towards constructing a cavity with a volume Bragg grating used for spectral control.

The input coupler was a short-pass filter coated for high reflectivity, over 99.9 %, at 1020-1200 nm and low reflectivity, less than 2 %, at 808-980 nm (all specifications are for 0^o incidence angle).

4.1 Linear cavity laser with a 2 mm long Yb:KYW crystal

In this section, a laser built with a 2 mm long N_g-cut Yb:KYW crystal and the method used for estimating the absorption of pump power are described.

The Yb:KYW had 5 % atomic doping and was broadband AR coated around 1040 nm on both sides. The crystal was placed in a water-cooled copper holder for cooling. The output coupler was a plano-concave mirror. The curved side had a radius of curvature of 50 mm and a coating giving 90 % reflectivity at 1000-1150 nm.

A lens with 35 mm focal length and AR coating in the range 650-1050 nm was used to focus the collimated pump beam into the Yb crystal. According to simulations, the pump beam waist $1/e^2$ radius was about 120 μm. The cavity length and the temperature of the pump laser were optimized for maximum output power at 44 A drive current, and stayed constant for all measurements. With a cavity length of about 33 mm and a pump laser temperature of 24.8 ^oC, the maximum output power was just under 6.8 W with a lasing threshold around 7.5 W of incident pump power, as shown in Fig. 4.1. The maximum optical efficiency, referring to output-to-pump power ratio, was just below 34 %. The average slope efficiency, referring to incident pump power, was about 54 %. According to simulations, the laser mode size was about 92 μm inside the Yb crystal when the effects of a thermal lens were neglected.

The simulations were conducted by using a software named *WinLase*. This software is designed to model and to analyze laser resonators or single pass systems based on the ABCD matrix formalism. This formalism, however, restricts the simulation of the resonating laser beam to an ideal gaussian beam.

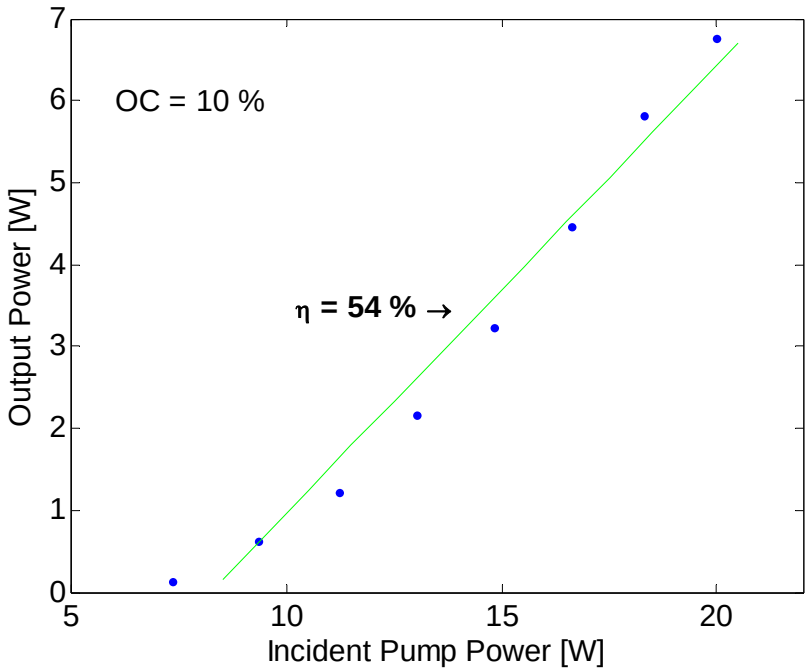

Figure 4.1: *Output power vs. incident pump power for the laser with a pump beam waist of about 120 μm.*

The absorbed pump power was estimated using the following method.

First, the pump power contained in the output at the output coupler was determined by subtracting the laser power in the far field from the total output power in a near field, since the pump beam was diverging much faster than the laser mode. Second, the output coupler was removed, and the pump power after the Yb crystal was measured. For pump powers below threshold, the data from the latest measurement multiplied with the transmission of the output coupler should be the same as the pump powers transmitted through the output coupler. This relation was used to estimate the transmission of the output coupler at the pump wavelength and to calculate the pump-power after the Yb crystal when lasing occurred. Thirdly, the Yb crystal was removed and the incident pump power was measured. It was assumed that other losses than absorption were in comparison so small they could be neglected. This assumption made it possible to determine the absorbed power as the difference in pump power before and after the Yb crystal.

The absorption shown in Fig. 4.2 is the absorbed-to-incident pump power ratio. The results show that more of the pump power was absorbed when the Yb:KYW laser was lasing. This is expected since there are more electrons available in the lower energy level ready to absorb the light when lasing. This is due to the depletion of the electrons in the upper laser level by the stimulated emission. The laser was optimized for maximum output power at the maximum pump power. However, the wavelength of the pump laser depends on its output power as shown in chapter 3. If the wavelength of the pump laser matches the highest absorption cross-section for Yb:KYW at

maximum pump power and the wavelength blue shifts towards regions with lower absorption cross-section when the pump power is decreased, it would cause a decrease in the absorption. This is considered to be the reason for the decrease in absorption with decreasing pump power.

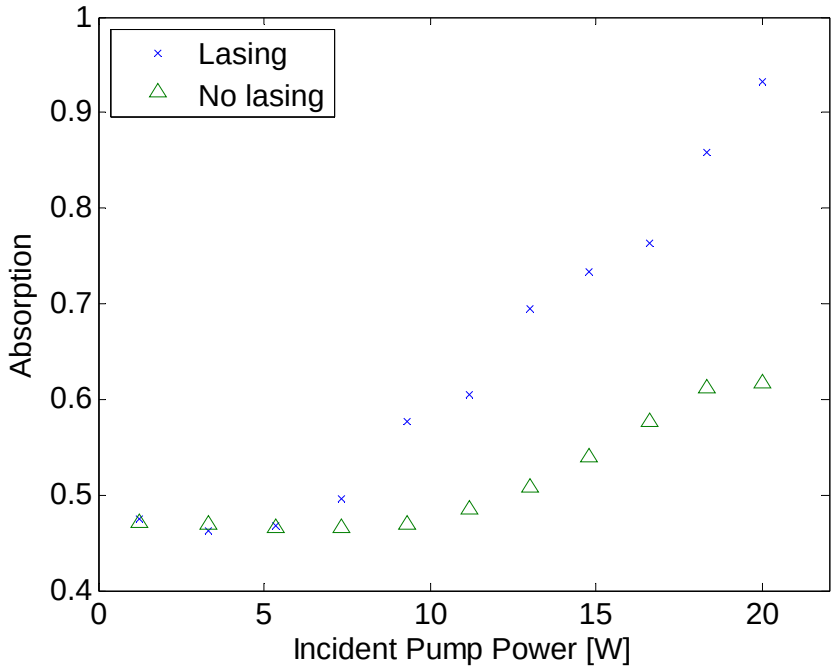

Figure 4.2: *Absorption vs. incident pump power, with and without laser cavity. Note that for the three points of lowest pump power, the laser is below threshold.*

The results are based upon the assumption that losses due to surface reflections and scattering are zero. Even if they are low compared to the absorption, it should be kept in mind that the actual absorption is lower than what is showed in Fig. 4.2.

4.2 Optimization of the output power of the laser with a 2 mm long Yb:KYW crystal

In this section, an experiment aiming to increase the output power of the laser described in the previous section is described. This was done by harder focusing of the pump beam in the Yb crystal. However, a smaller focal spot of the pump and a smaller mode size also increases the strength of the thermal lens in the crystal. This could have a negative effect on the stability and on the output power of the laser, especially for the higher powers.

The focusing was changed by replacing the lens (f = 35 mm) for focusing the pump beam to a similar one with 30 mm focal length. According to simulations, with the 30 mm lens the beam waist $1/e^2$ radius inside the Yb-crystal was about 100 μm.

Now, with a cavity length of about 28 mm, the maximum output power was about 7.8 W with a threshold just below 5 W incident pump power, as seen in Fig 4.3. When comparing the output power with the 6.8 W of output power achieved with the laser in the previous section, it is clear that a harder focus increased the output power. According to simulations the mode size was about 93 μm inside the Yb crystal when the effects of a thermal lens were neglected. The laser had an average slope efficiency, in terms of incident pump power, of about 58 %. The curve seen in Fig. 4.3 is, however, not a straight line. The slope efficiency is increasing until a point, around 17 W incident pump power, after which it appears to decrease. The increase can be explained by the increase of absorption with increasing pump power as described in the previous section. The decrease in the slope efficiency, even though the absorption should be increasing, is considered to be due to an increased strength of the thermal lens, reshaping the mode resonating in the cavity and having a negative effect on the maximum power the system can deliver.

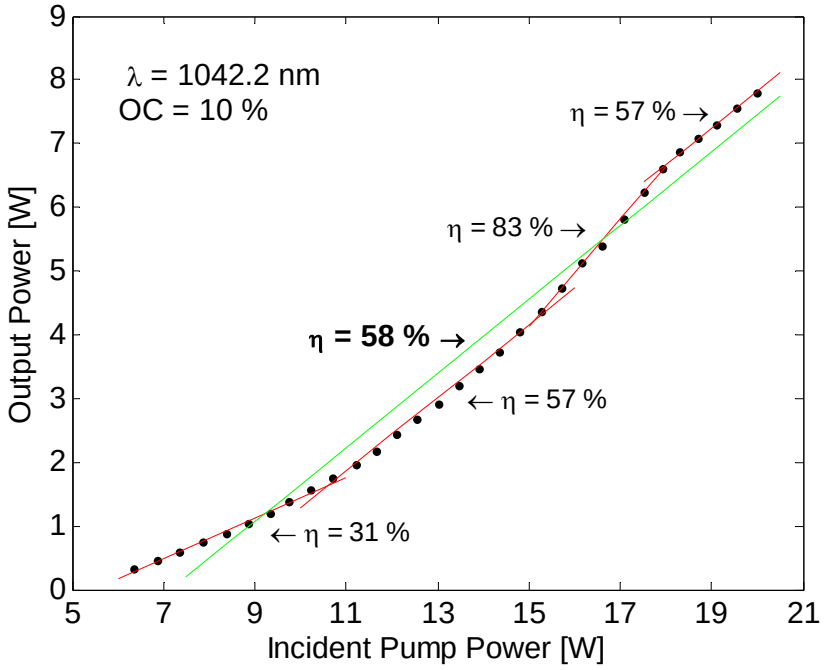

Figure 4.3: *Output power vs. incident pump power for the laser with a pump beam waist of about 100 μm. The green line is a linear fit, to the whole curve, with slope efficiency about 58 %. The red lines, with corresponding slope efficiencies, are linear fits to different parts of the curve.*

Even if the slope efficiency gives a lot of information about how the laser behaves, it is the optical efficiency that reveals how efficient the laser is. As shown in Fig. 4.4, the highest optical efficiency, referring to the output-to-input power ratio, achieved was about 39 % obtained at maximum power. The role-off is considered to be due to thermal lensing.

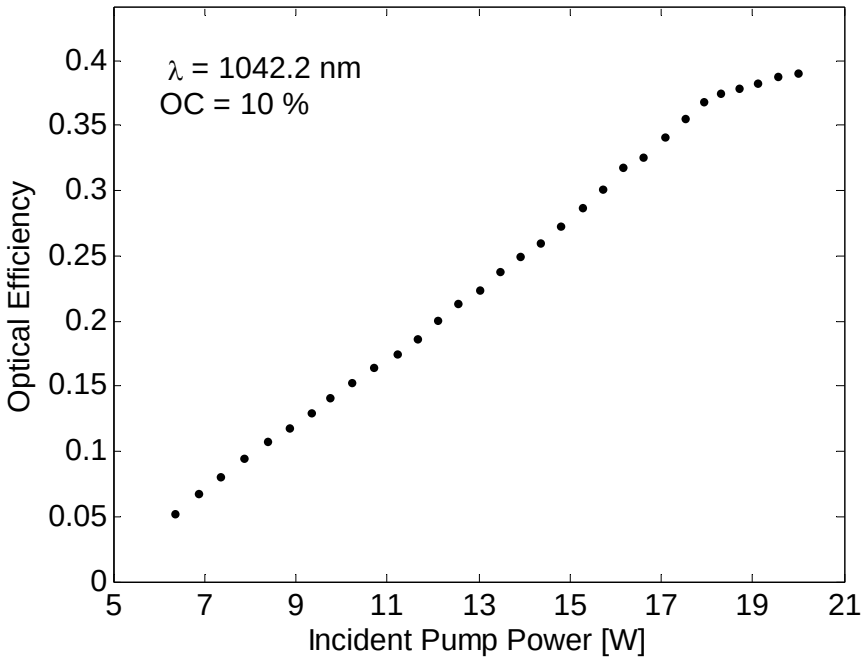

Figure 4.4: *Optical efficiency vs. incident pump power.*

A spectrum analyzer (Hewlett-Packard 86140A) with a resolution bandwidth of 0.07 nm was used to analyze the laser spectrum at 20 W of incident pump power (Fig. 4.5). The spectrum shows lasing on several longitudinal modes around a wavelength of 1042.2 nm with a bandwidth spanning from around 1041.9 nm to 1042.4 nm. The spectral power distribution was observed to fluctuate.

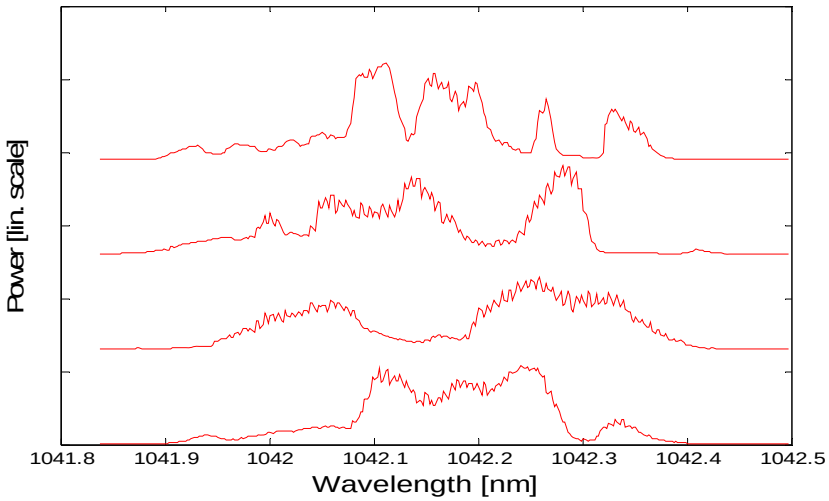

Figure 4.5: *Four spectra of the output laser beam taken at different times.*

4.3 Linear cavity laser with a 3 mm long Yb:KYW

The second laser was built with the same optics as the laser described in section 4.2 except the output-coupler was switched to a similar one with a coating of 85 % reflectivity instead of 90 %. The gain medium used was a 3 mm long N_p cut Yb:KYW crystal with 5 % atomic doping and AR coating for the range 920-1300 nm. The crystal was placed in a water cooled copper holder for cooling.

After the system was optimized, with a cavity length of about 34 mm, the maximum output power was about 6 W with average slop efficiency about 54 % as shown in Fig. 4.6. The highest optical efficiency, referring to the output-to-input power ratio, was just below 30 % at maximum pump power. Compared to the laser in the previous section the output power is lower, 6 W compared to 7.8 W. It is considered that the focus of the pump was not optimal for this crystal length. This caused some absorption of the laser mode in the unpumped parts of the Yb:KYW crystal.

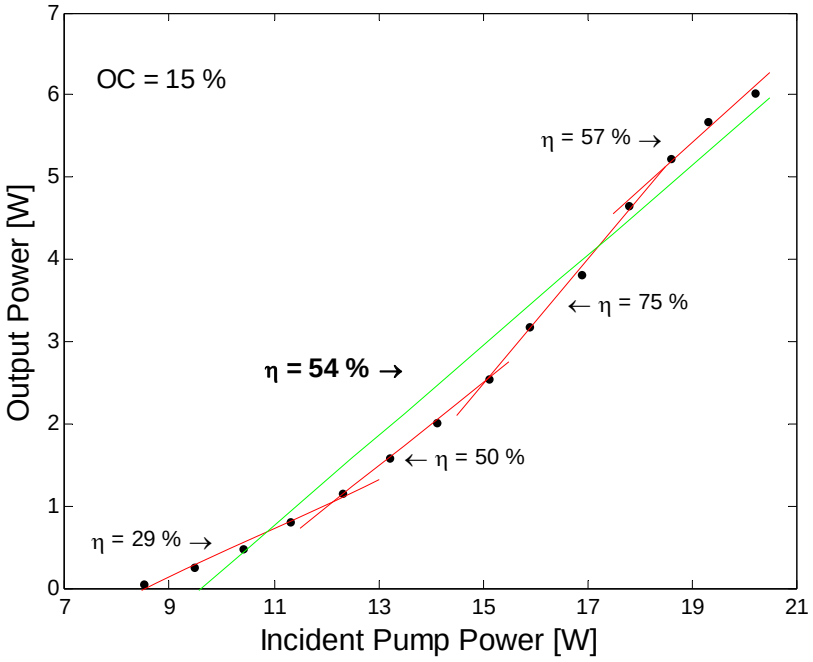

Figure 4.6: *Output power vs. incident pump power. The green line is a linear fit, to the whole curve, with slope efficiency about 54 %. The red lines, with corresponding slope efficiencies, are linear fits to different parts of the curve.*

4.4 Folded cavity laser with a 3 mm long Yb:KYW

In this section, a laser constructed with a folded cavity is described. The reason for designing a folded cavity was to be able to use a VBG for locking the laser spectrum without pumping through it, as described in Sec. 5.2.

This laser was built with the same output (R = 90 %) and input coupler as the laser described in Sec. 4.1. The gain-medium used was a 3 mm long N_p cut Yb:KYW crystal with 5 % atomic doping and AR coating for the range 920-1300 nm. The crystal was placed in a water cooled copper holder. The input coupler was placed at an angle of about 11^o to the incident pump beam. A plano-plano highly reflecting mirror was used to complete the cavity as shown schematically in Fig. 4.8. The highly reflecting mirror had a reflectivity of 99.95 % in the region 970-1430 nm. A lens with 35 mm focal length and AR coating in the range 650-1050 nm was used to focus the pump beam into the Yb crystal.

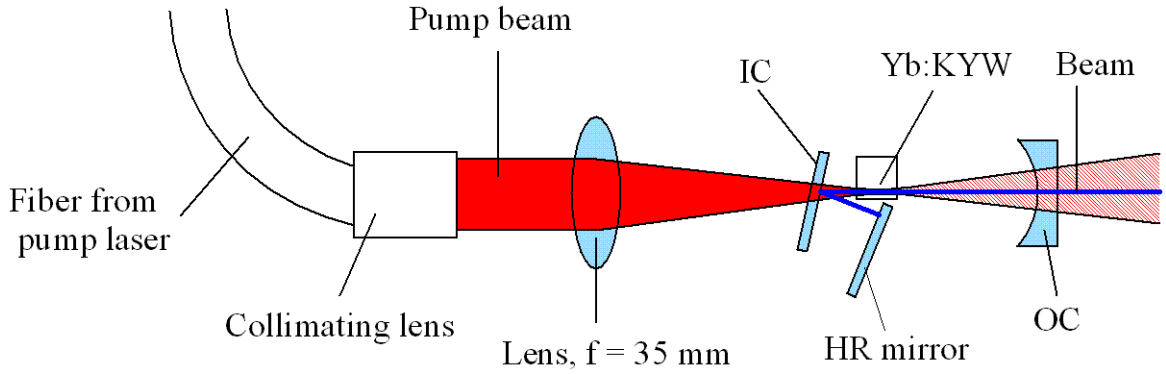

Figure 4.8: *Schematic drawing of the laser setup.*

According to simulations, the $1/e^2$ radii of the laser mode and the pump beam waist inside the crystal were about 110 μm and 120 μm, respectively.

Placing the input coupler at an angle shifted the low reflectivity region towards shorter wavelengths. This resulted in lowering of the maximum incident pump power from just above 20 W for normal incidence angle to just above 17 W. In Fig 4.9, both the incident pump power and the pump output power with respect to current are shown. It can be observed that the slope efficiency, referring to power-to-current ratio decreases for the currents higher than approximately 35 A, after which the spectrum of the pump is redshifted out of the low reflectivity region of the input coupling mirror.

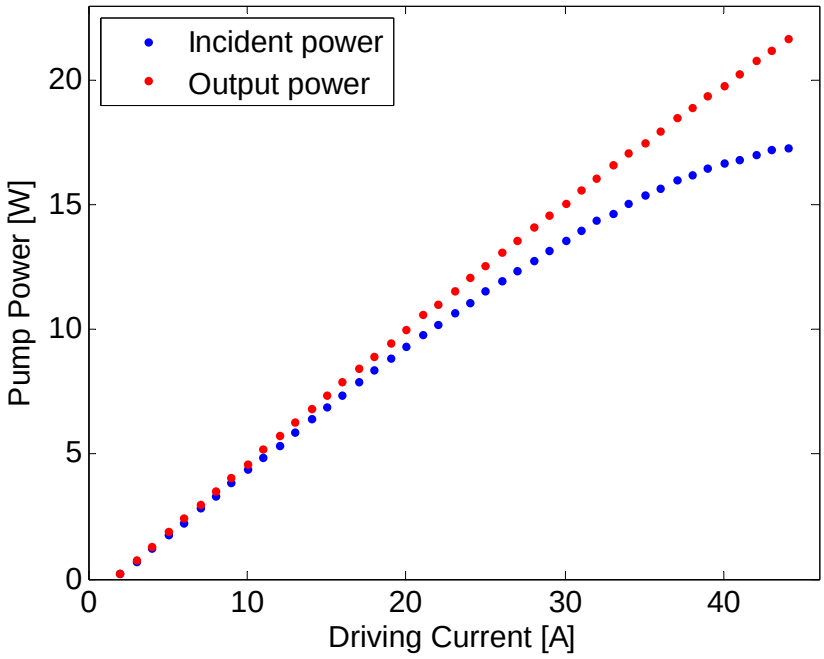

Figure 4.9: *Pump power incident on the Yb:KYW crystal vs. pump laser drive current.*

The maximum laser output power was about 3 W with an optical efficiency of about 17 %. The threshold was about 11 W incident pump power as shown in Fig. 4.10. The lower output power (3 W) compared to the laser in the previous section, about 4 W at 17 W of incident pump power, can primarily be explained by the larger focal spot required to match the larger mode inside the crystal. Since the volume of the pump in the Yb crystal increased, population inversion may not have been achieved throughout the crystal, with absorption of the laser light as a result.

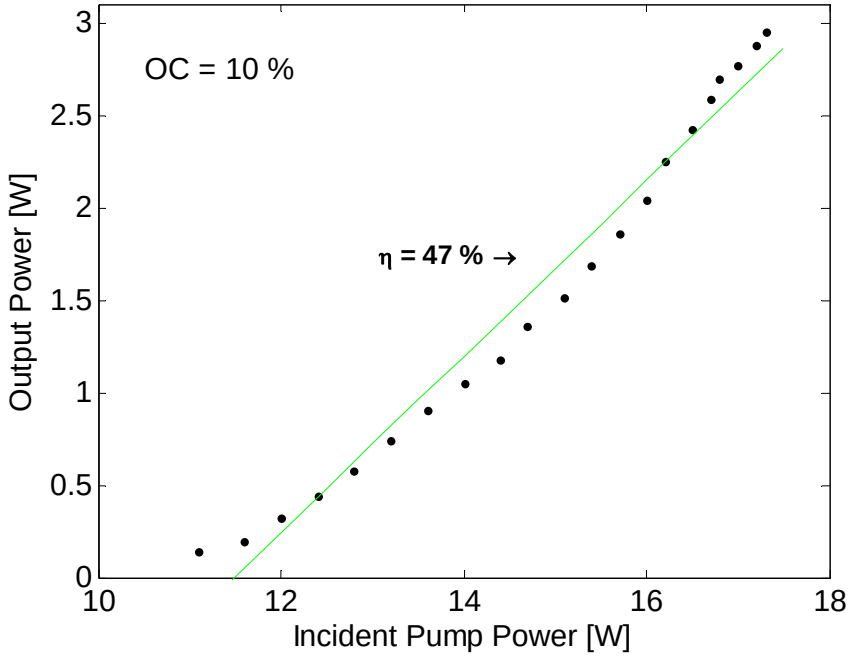

Figure 4.10: *Laser output power vs. incident pump power. The green line is a linear fit, to the whole curve, with slope efficiency of about 47 %.*

After these initial Yb:KYW laser experiments, the cavities were rebuilt using volume Bragg gratings for spectral control. These experiments are described in the two following chapters.

5 Lasers with the long VBG – thermal effects

The goal with the experiments described in this chapter was to lock the laser spectrum with a volume Bragg grating (VBG). Attempts were made with both a linear cavity, where the gain medium was pumped through the VBG, and with a folded cavity. The reason for not using the VBG as an output coupler was to have the option to try output couplers with different reflectivities in later Q-switching experiments. The degree of output coupling is a parameter used to achieve the desired pulses when Q-switching.

The VBG used in these experiments was 9.7 mm long. According to measurements conducted at low power, the reflectivity was 99.4 % at 1029 nm with a bandwidth of around 0.2 nm at FWHM [16]. The grating was broadband AR coated around 1030 nm. The VBG was mounted on top of a mirror mount attached with nail polish. This volume Bragg grating had a more brownish color than what is usual for volume Bragg gratings in general.

The results presented in this chapter showed lower output power compared to the lasers built with a dielectric mirror instead of a VBG. The spectrum red shifted with increasing pump power and both spectral broadening and side peaks were observed. Measurements of the surface temperature showed that the VBG absorbed both the pump and the laser. It was concluded that the absorption in the VBG caused the unexpected poor performance of the lasers and it was decided that this particular VBG was not to be used as a cavity end mirror in further experiments.

5.1 Linear cavity laser with the VBG as input coupler

The first experiment was to use the VBG instead of the input coupler in the laser-system described in Sec. 4.2. As shown schematically in Fig. 5.1, the pump beam was focused through the VBG into the Yb crystal. The VBG was positioned so that the laser mode was incident upon approximately the center of the end surface.

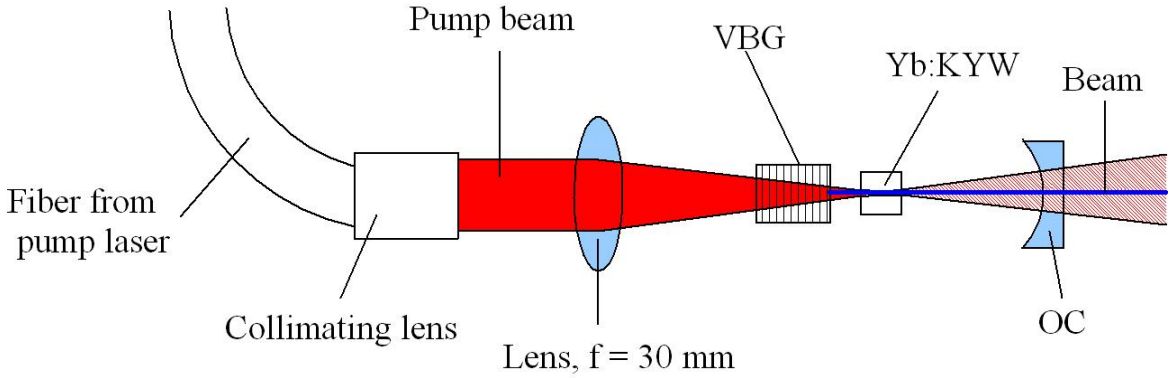

Figure 5.1: *Schematic drawing of the setup.*

Fig. 5.2 shows the laser output power versus pump power. That the highest measured output power was just below 1.8 W with a lasing threshold about 9 W incident pump power. The error

bars show the observed fluctuations during the measurement. The output power was remarkably low compared to the 7.8 W achieved with the laser with a dielectric mirror as input coupler (Sec. 4.2). The reasons for the low power are investigated further on in this chapter.

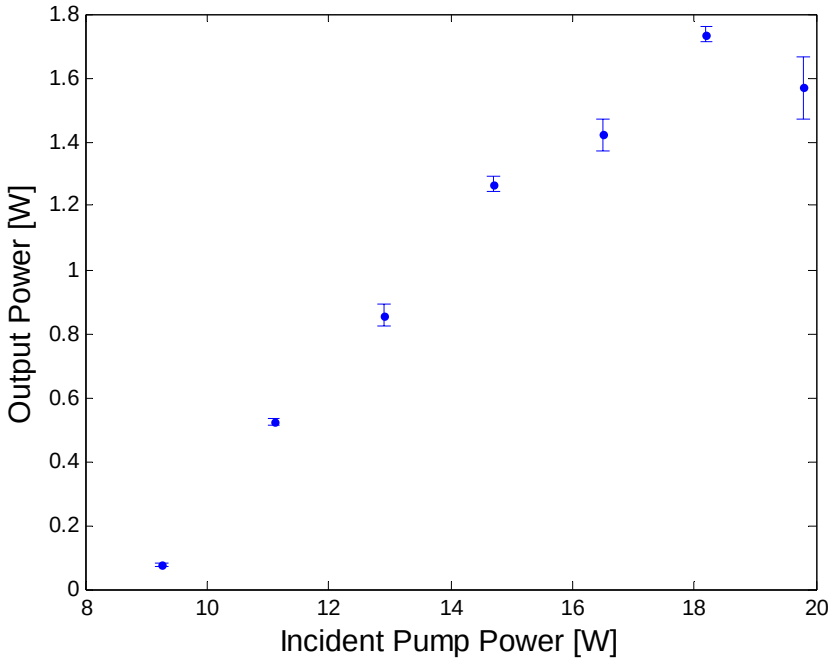

Figure 5.2: *Output power vs. incident pump power for the linear cavity VBG laser. The error bars show observed fluctuations and the dots show the median value.*

A spectrum analyzer (Hewlett-Packard 86140A) with a resolution bandwidth of 0.07 nm was used to analyze the laser spectrum. As can be seen in Fig 5.3 the spectrum was redshifted with increasing pump power. As the pump power reached about 18 W, side peaks were also observed in the spectrum. They were redshifted with respect to the main peak and fluctuated in both amplitude and wavelength. The shift of the laser peak is attributed to heating of the VBG due to absorption of pump and laser light. When the beam cross section was observed with the naked eye on an IR viewing card, it was observed that the laser was lasing on multiple transverse modes.

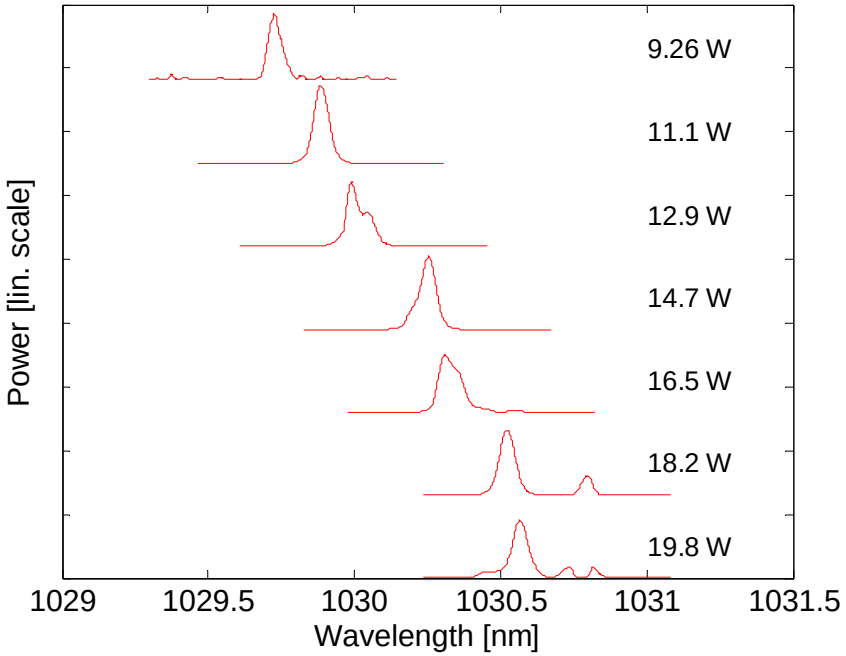

Figure 5.3: *Spectrum of the linear cavity VBG laser at different incident pump powers.*

Overall heating of the grating would cause an increase of the grating period in the VBG through thermal expansion, resulting in a redshifted spectrum as can be seen for the main peak in Fig. 5.3 where it shifts continuously with increasing pump power i.e. absorbed power. The appearances of side peaks, however, indicate that the grating periods were not equally increased throughout the VBG. The intensity of both the pump and the laser were highest at the end surface closest to the Yb crystal. This is considered to cause an unevenly distributed temperature in the VBG resulting in the low performance (below 1.8 W output power) of the laser compared to the laser with a dielectric input coupler (around 7.8 W output power) described in Sec. 4.2.

Thermal effects for nonresonant beams

A PT-100 temperature sensor was placed on top of the VBG to measure the temperature for incremental pump power. For each pump power, the temperature was measured after 3 minutes for thermal equilibrium to be reached. As shown in Fig 5.4, the temperature increased from room temperature in a smooth curve up to approximately 96 ^{o}C.

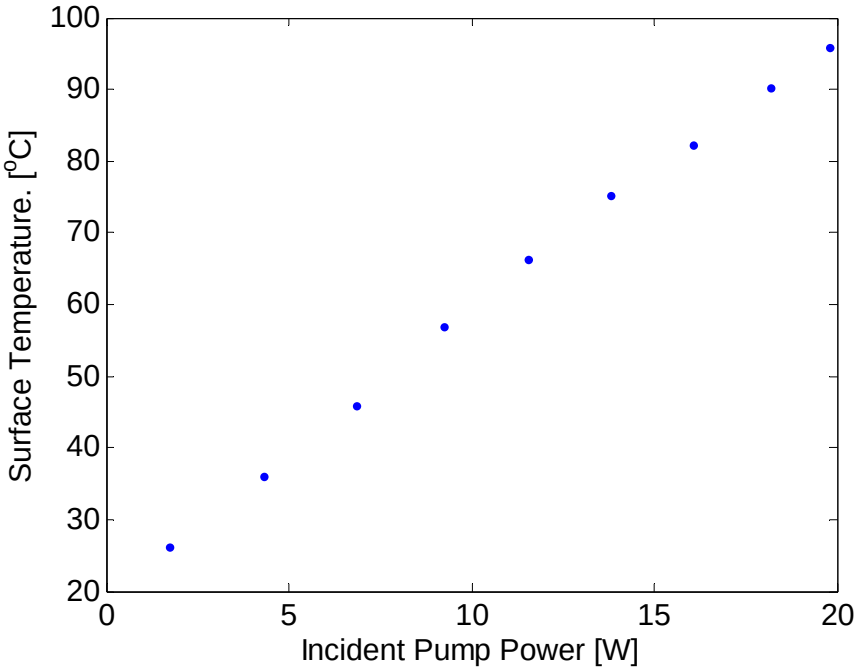

Figure 5.4: *Surface temperature of the VBG vs. incident pump power.*

To investigate whether the measured temperature was due to increased temperature in the VBG or absorption of scattered light in the PT-100 sensor, the VBG was observed with an infrared camera (AGA Thermovision 780).

The thermal images are shown in Fig. 5.5 and indicate that the VBG becomes hot during the pumping, while there is no indication of the PT-100 sensor being warmed up by the pump. Thus it was concluded that the measured temperature was equal to the surface temperature of the VBG. The lenses used with the camera was not designed for this application, so the camera was placed closer than the focal point. This lowered the resolution of the images.

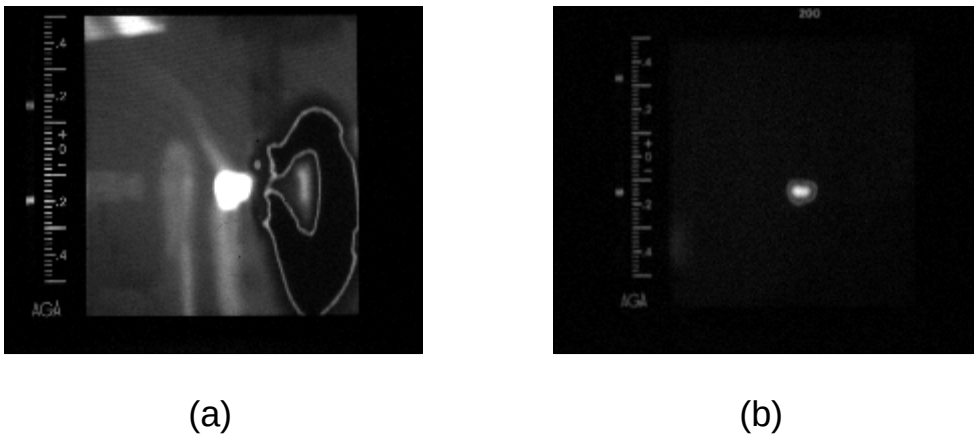

(a) (b)

Figure 5.5: *Thermal images of the VBG. The two images (a) and (b) are taken at different exposure levels.*

To further investigate the heating, an interferometer measurement was made. As depicted in Fig. 5.6, the measurement was conducted with a laser beam from a HeNe-laser (wavelength 633 nm) which was sent through the VBG in the opposite direction of the pump beam. The reflections from the end surfaces interfered with each other and the change in the interference pattern with increasing pump power was recorded. In Fig. 5.7 two images from the interference measurement is shown. It was observed that 29 interference minima appeared in the centre of the beam during the increasing of pump power. This shows that the single pass optical path length increased by about 9 μm as the pump power was turned up to maximum. With a refractive index of $n_0 = 1.49$, a thermal expansion coefficient $\alpha = 8.4$ ppm/K, see [17] and references therein, the increase in temperature can be calculated using the following relation:

$$\alpha \Delta T = \frac{\Delta L}{L} \tag{5.1}$$

Here, L is the length of the VBG, ΔL is the increase in VBG length and ΔT is the increase in temperature. It was calculated that the increase in optical path length would correspond to an average increase in temperature around 74 ^{o}C. The measurement was conducted in room temperature, about 20 ^{o}C, meaning that the VBG increased to an average temperature of about 94 ^{o}C. This result corresponds well to the increase in surface temperature that was measured with a PT-100 temperature sensor.

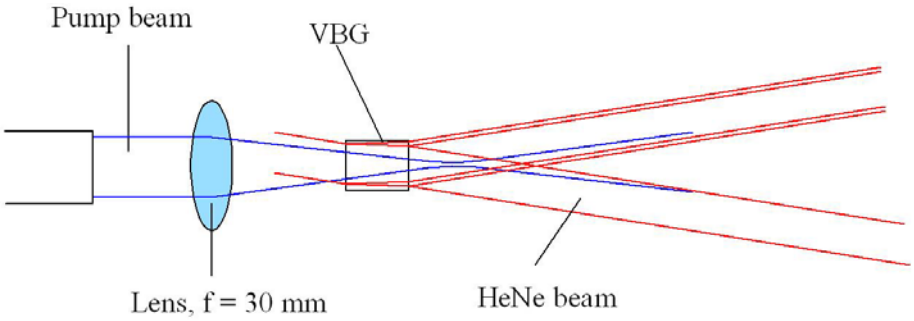

Figure 5.6: *Schematic drawing of the interferometer measurement.*

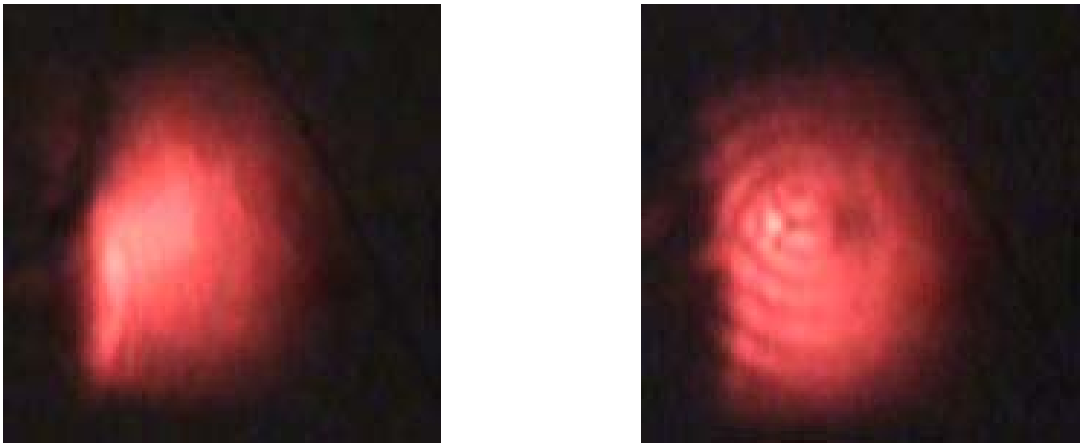

(a) (b)

Figure 5.7: *Images from the interference measurement. Image (a) shows the interference pattern before the pump laser was started. Image (b) shows the pattern when the pump output power is about 20 W.*

5.2 Folded cavity – thermal effects for resonant beams

In this section, a laser constructed with a folded cavity is described. The reason for designing a folded cavity was to be able to use a VBG for locking the laser spectrum without pumping through it and thereby absorb pump light.

The setup is similar to the one described in Sec. 4.4, but the HR flat end mirror was replaced by the VBG as shown schematically in Fig. 5.8. Also, the output coupler (ROC = 50 mm) was replaced with a similar one with coating for 85 % reflectivity. The VBG was positioned so that the laser mode was incident upon the end surface close to one of the edges. According to simulations, the $1/e^2$ radii of the laser mode inside the crystal and at the end surface of the VBG were about 105 μm and 90 μm, respectively.

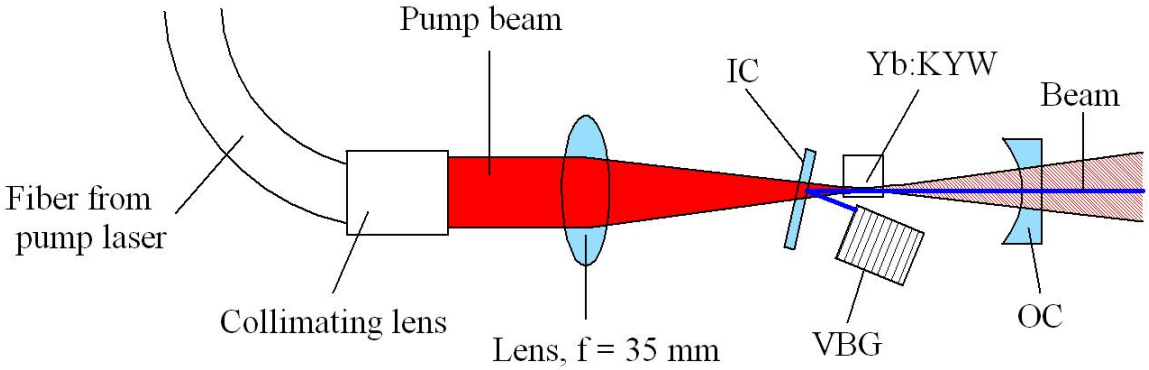

Figure 5.8: *Schematic drawing of the folded cavity.*

In Fig. 5.9, measured data of the output power through the output coupler as well as the power passing through the VBG is shown. At maximum pump power, the powers through the

output coupler and the VBG were around 1.1 W and 0.5 W, respectively. The measured output power through the output coupler is lower compared to when the laser was built with an HR-mirror instead of the VBG (Sec. 4.4).

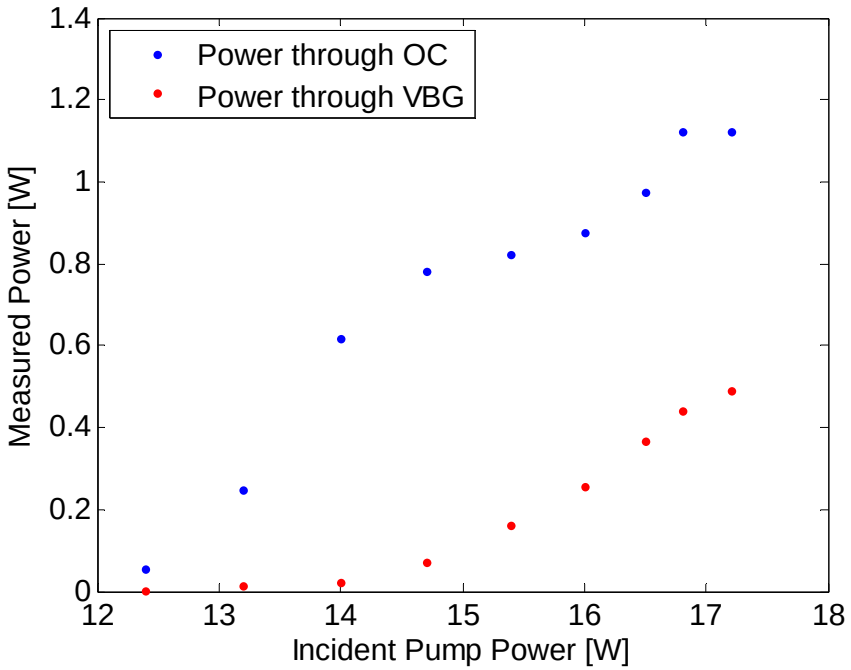

Figure 5.9: *Output power vs. incident pump power.*

Based on the measurements of the output power through the ordinary output coupler and the VBG, the reflectivity of the VBG was calculated. The data is shown in Fig. 5.10 versus both the one way circulating laser powers incident on the VBG and the intensity I_0 incident on the VBG. Here I_0 is the intensity in the center of the beam. One can observe that the reflectivity of the VBG decreases from 99.4 %, measured at low powers, to about 94 % as the intensity incident upon it increases.

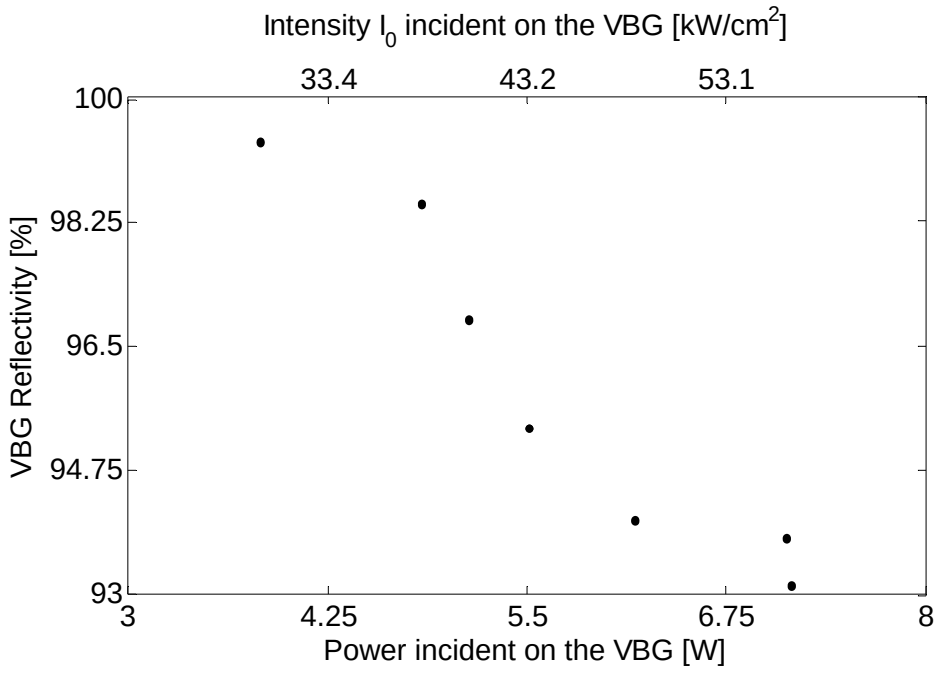

Figure 5.10: *Reflectivity of the VBG vs. incident laser power (bottom) and incident intensity I_0 (top).*

The surface temperature of the VBG was measured using a PT-100 sensor on top of it in the same way as described in Sec. 5.1. As shown in Fig. 5.11 the temperature rose from room temperature to around 54 ^{o}C.

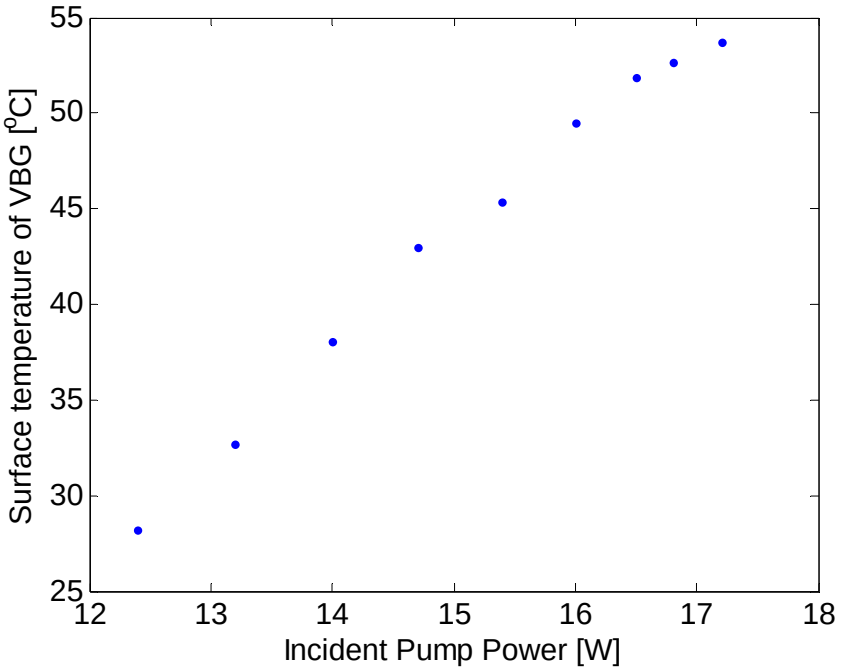

Figure 5.11: *Surface temperature of the VBG vs. incident pump powers.*

The spectrum of the beam exiting the output-coupler was again measured with the spectrum analyzer. It was observed, as shown in Fig.5.12, that the spectrum was redshifted and broadened with increased pump power. It was also observed that the main peak fluctuated in wavelength when the pump power reached around 15 W.

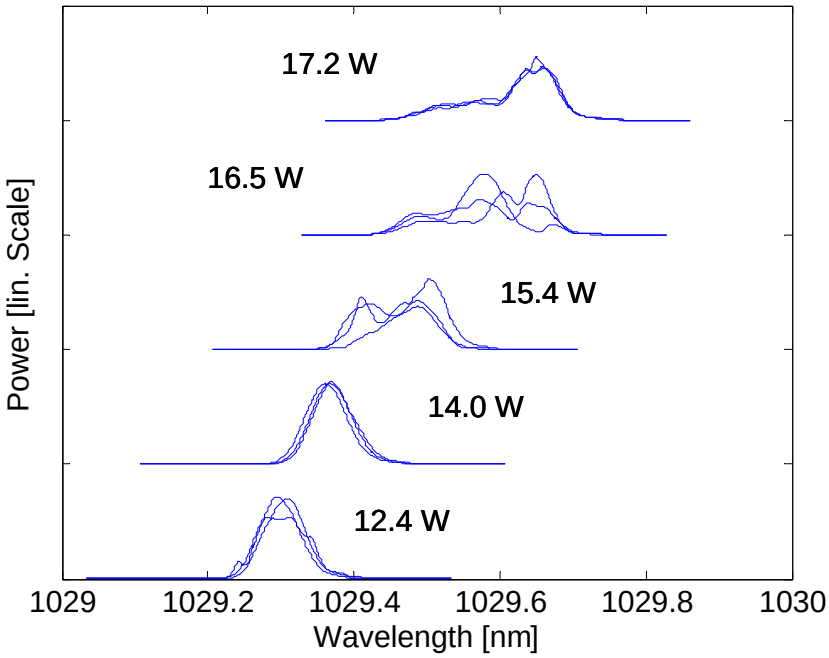

Figure 5.12: *Normalized spectra of the beam exiting the OC for different incident pump powers. For each pump power three spectra are plotted on top of each other.*

5.3 Discussion

In Sec. 5.1, the grating was used as an input coupler, with the pump passing through it into the Yb:KYW. The output power was about 1.8 W which is considerably lower than the 7.8 W of output power achieved with a dielectric mirror as input coupler (Sec. 4.2). The spectrum of the laser (Fig. 5.3) shows an overall redshift as the pump power increases. When the pump power reached about 18 W, side peaks appeared and the spectrum broadened. It was then investigated how the grating was affected by the nonresonant pump beam only. Two independent measurements showed that the temperature had increased by approximately 75 ^{o}C as the pump power was increased to about 20 W, and that the grating was deformed by the absorbed pump power. It is concluded that this particular grating is absorbing the pump beam too strongly and is not suitable for use as an input coupler.

In Sec. 5.2, a folded cavity was designed to avoid exposing the volume Bragg grating to the pump beam. Still, the output power (about 1.1 W), through the output coupler, was lower than in the cavity with a dielectric end mirror (about 3 W, see Sec. 4.4). It was observed, however, that the power leaking out through the grating increased to about 0.5 W, as the pump power increased. This data was used to calculate how the reflectivity of the grating changed as the laser power incident upon it increased. The results (Fig. 5.10) show that the reflectivity decreased from 99.4 % (measured at low power (16)) to about 93 %. The spectrum (Fig. 5.12) show an overall redshift and broadening as the pump power increases. The surface temperature increased from approximately 20 ^{o}C to 55 ^{o}C.

Next, calculations were made to investigate how the intensity of the laser was distributed along the propagation axis when reflected in the grating. An equation describing the intensity of the laser mode throughout the grating can be found in [18]. After correcting typographic errors, the normalized average intensity inside the grating along the propagation direction, z, is given by:

$$I(z) = \frac{1}{\cosh^2\left(\tanh^{-1}\sqrt{R}\right)} \cdot \cosh\left(2\tanh^{-1}\sqrt{R}\,(d-z)/d\right) \tag{5.1}$$

Here, R is the peak reflectivity and d is the thickness of the grating. In Fig. 5.13, the intensity calculated with Eq. 5.1 with the data for this particular VBG is shown. One can see that the intensity is highest at the end surface closest to the Yb:KYW crystal and that it decreases approximately exponentially.

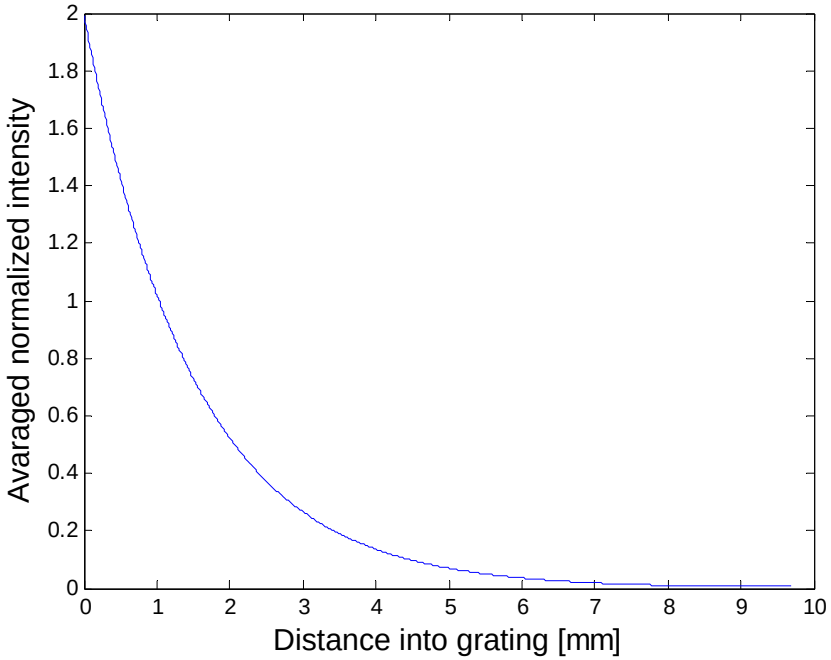

Figure 5.13: *Averaged normalized intensity at different distances into the grating. The intensity of 1 equals to the intensity incident upon the grating.*

It was concluded that the grating absorbed the laser mode, causing thermal load on the grating. Since the intensity of the mode decreased approximately exponentially in the grating, the temperature became unevenly distributed along the propagation axis. This resulted in different thermal expansion and hence, resulted in a longitudinal chirp which caused a decrease in both reflectivity and spectral selectivity.

Future work

It would be a good idea to find a reliable method of measuring the absorption of volume Bragg gratings. One way could be to place the grating on a thermoelectric cooler with temperature control while transmitting a laser beam through the grating and measure the current required to keep the temperature constant. The procedure should be repeated for a piece of glass with known absorption. By comparing the results from the two measurements, the absorption of the grating can be determined.

When the absorption of the gratings in known, less absorbing gratings can be compared to the highly absorbing grating, and using the results presented in this chapter, the limitations of the less absorbing gratings can be estimated.

It would also be interesting to construct a laser with the highly absorbing grating and measure the changes in optical path length (OPL) for different parts of the grating along the propagation axis. This could be done with an interference measurement conducted from the side of the grating. The results would be a map of the optical path length changes, which can be compared to the predictions of the grating chirp based on the theoretical intensity distribution made above.

6 Lasers with the short VBG

In this chapter, experiments to lock the laser spectrum with a second shorter VBG, generation of pulses through passive Q-switching, second harmonic generation (SHG) and sum frequency generation (SFG) are described.

The VBG used in these experiments was 2.8 mm long. Compared the longer grating used in the previous chapter, this grating looked more transparent. For that reason, it was assumed that it was less absorbing. As the results will show, this assumption was correct. According to measurements conducted at low power, the reflectivity of the grating was around 99.5 % at 1028.8 nm with a bandwidth around 0.5 nm at FWHM [16]. The grating was also broadband AR coated around 1030 nm. The VBG was mounted on top of a mirror mount attached with nail polish, as in the previous experiment.

In all experiments described in this chapter, a 3 mm long N_p-cut Yb:KYW crystal with 5 % atomic doping and AR coating for the range 920-1300 nm was used.

6.1 Linear cavity cw laser

The first goal was to build a laser with a VBG as an input coupler in the same way as described in Sec. 5.1.

The input coupler in the laser described in Sec. 4.3 was replaced by the VBG. As before, the length of the cavity and the crystal position was adjusted to get maximum output power, leading to a cavity length about 33 mm. The distance between the Yb crystal and the VBG was around 3 mm.

The maximum measured output power, shown in Fig. 6.1, was about 5.1 W with an optical efficiency of about 26 % and a threshold of about 8 W incident pump power. The laser had average slope efficiency, in terms of incident pump power, of about 51 %. When the cavity was constructed with a dielectric mirror as input coupler (Sec. 4.3) the output power was about 6 W, so there was a slight decrease in maximum output when using the VBG. The spectrum of that laser was, however, not locked so lasing occurred at a wavelength of different gain. This means that the optimal level of output coupling is different for the two lasers. Compared to the 1.8 W of output power achieved with the longer VBG (Sec. 5.1), it appears that this VBG was less absorbing and that no thermal problems occurred.

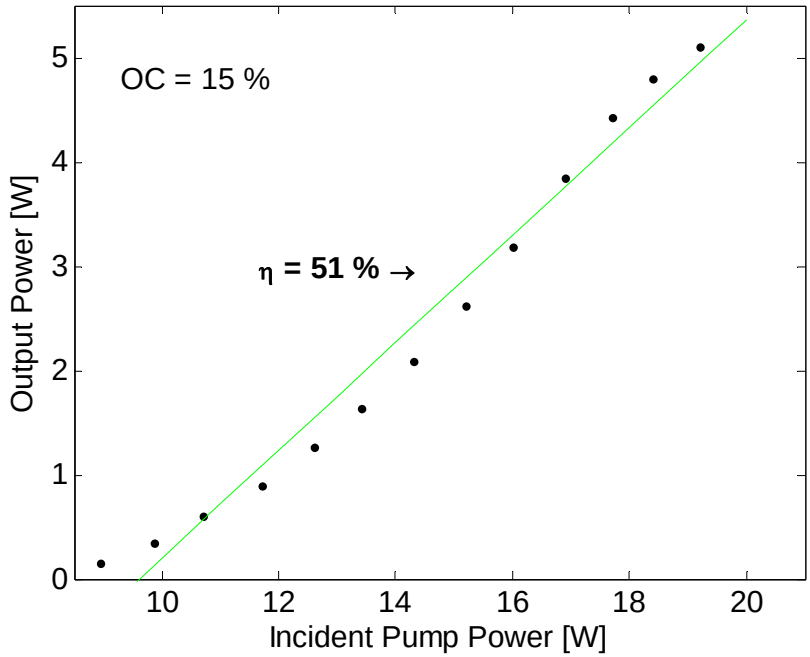

Figure 6.1: *Laser power vs. incident pump power. The green line is a linear fit, to the whole curve, with slope efficiency about 51 %.*

In Fig. 6.2 the spectrum of the laser at different pump powers is shown. It can be observed that the spectrum is again redshifted with increasing pump power. The presence of multiple peaks in the spectra indicates that oscillation on several longitudinal modes occurred with a frequency separation about 24 GHz. The mode separation corresponds to the optical length of the Yb crystal, which indicates that the crystal was partly acting as a Febry-Pérot etalon, limiting the allowed modes in the cavity. Comparing with the spectrum from the laser with the longer VBG (Fig. 5.3), this spectrum shows no appearance of side peaks or spectral broadening.

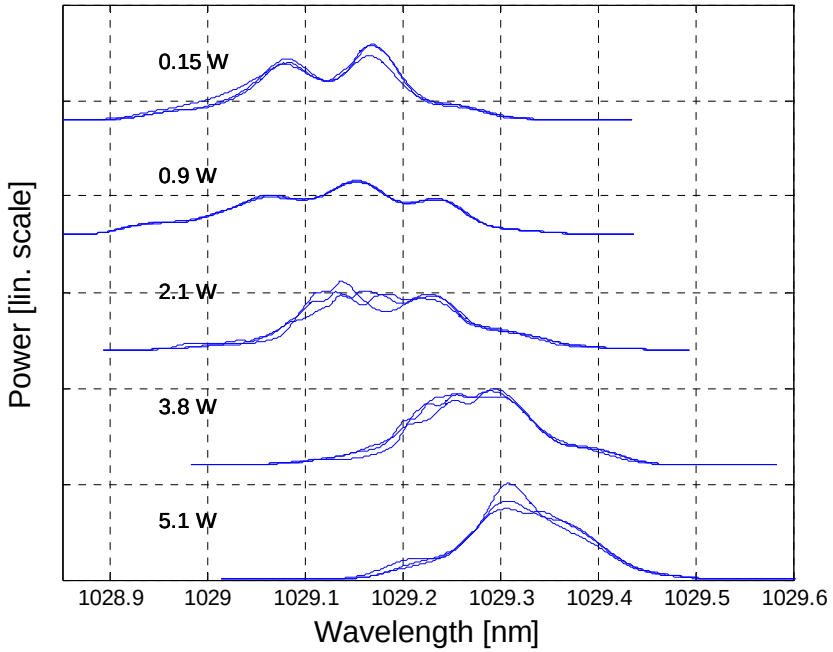

Figure 6.2: *Spectra of the VBG-locked laser for different output powers.*

To investigate how the output power and the spectrum of the laser behaved over time when it was operated at maximum pump power, measurements were made every 5 minutes over a time period of 45 minutes. The results are shown in Fig. 6.3 and indicate a good stability in the output power. The difference in the highest and lowest measured power was below 1 %.

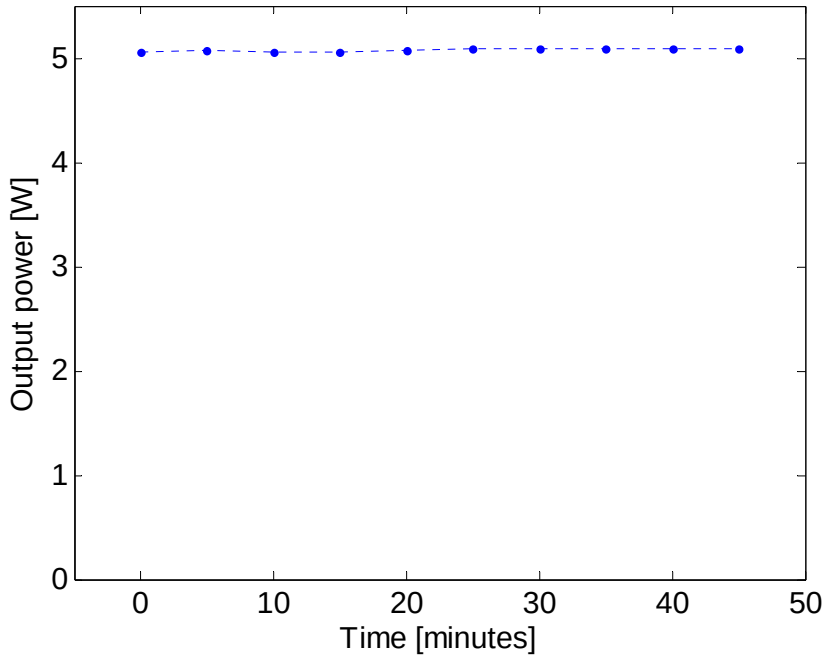

Figure 6.3: *Output power vs. time when the laser is running at maximum pump power.*

In Fig. 6.4 the measurements of the spectrum are shown. One can observe that the wavelength distribution experiences some redshift over time. This together with the observed redshift of the spectrum with increasing pump power indicates that there is also absorption in this VBG. The absorption appears, however, not to be enough to cause the performance lowering effects that were observed in the experiments described in chapter 5.

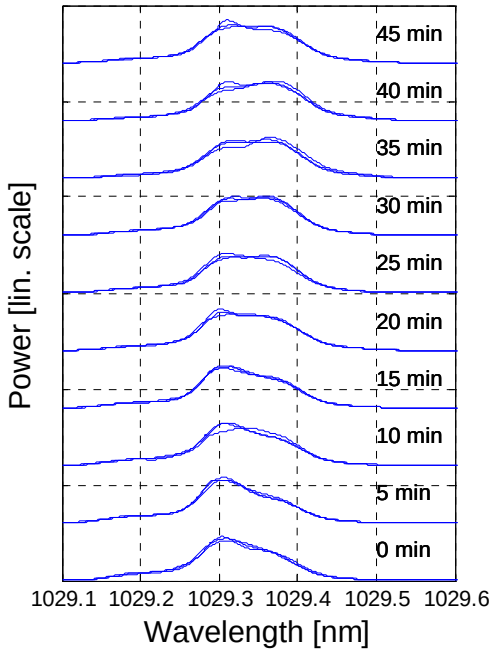

Figure 6.4: *Normalized spectra at different times after laser start-up when operated at maximum pump-power.*

6.2 Pulsed laser

In this section the experiments aiming to modify the laser to a pulsed laser is described.

To create a passively Q-switched laser, a Cr^{4+}:YAG crystal was placed inside the cavity of the laser described in the previous section. A schematic drawing is depicted in Fig. 6.5. The initial transmission of the chosen Cr:YAG was 94 % for 0^{o} angle of incidence. It was placed in Brewster's angle (61^{o} for YAG) which leads to an effective initial transmission of 93 %.

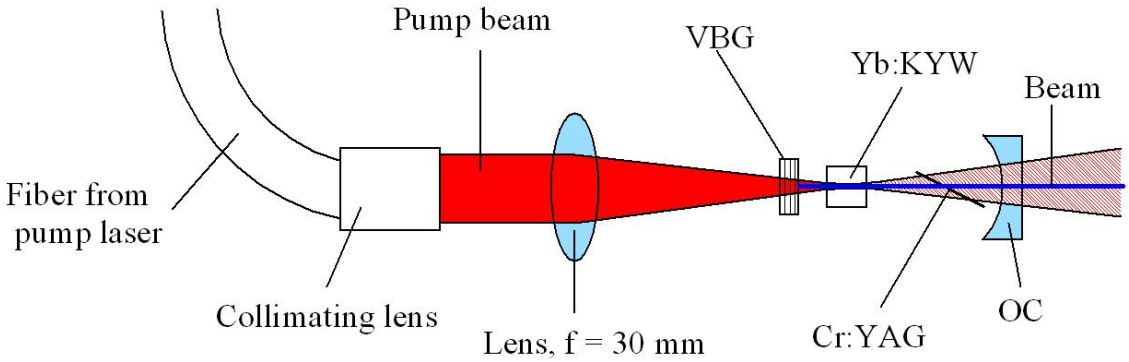

Figure 6.5: *Schematic drawing of the setup.*

Experiments were conducted to find the Cr:YAG that resulted in the highest peak power. The investigated Cr:YAG crystals had initial transmission of 98 %, 96 %, 94 % 90 % and 86 % at normal angle of incidence, respectively. The crystals were inserted into the cavity in Brewster's angle.

Q-switching was achieved with the three crystals of highest initial transmission. The largest peak power was achieved with the Cr:YAG that had the initial transmission of 94 %. With the crystals of initial transmission 90 % and 86 %, lasing was only achieved for a few pulses. After these events, the Yb:KYW crystal needed to be translated in a transverse direction for the laser to work in cw mode again (with the Cr:YAG removed). This indicates that the pulse energy was too high for the coating of the Yb:KYW crystal and caused damage to it (Sec. 6.5).

At one point, when the output coupler of the laser was adjusted to find a better overlap between the mode and the pump, the Cr:YAG, with the initial transmission of 94 %, cracked into several pieces. The circulating laser power was at that time around 7 W for one direction. One of the pieces was used for the further experiments since this was the crystal that was desired to be used in the setup. It is believed that the crack was caused by thermal induced stress in the crystal.

During the experiment, it was observed that the average output power increased when the pump laser drive current was increased but the pulse peak power decreased. When the incident pump power reached about 17 W, the laser started lasing in cw mode and fluorescence that to the naked eye appeared as red was emitted from the Cr:YAG. The reason for this behavior is probably that of the remaining pump beam that is not absorbed in the Yb crystal is bleaching the saturable absorber, in addition to the laser itself.

Since the conversion in a nonlinear process depends on the peak power and not the average power, it was concluded that the laser should not be operated at maximum pump power. The temperature of the pump laser was, however, optimized at maximum pump power. To increase the absorption at lower pump power, the temperature of the pump laser needed to be increased. It was decided to increase the temperature of the pump laser from 24.8 ^{o}C to 29 ^{o}C. It is likely that further increase of the temperature would have provided even higher peak power, but it also decreases the life time of the pump laser. In Fig. 6.5, the peak power and average power of the

Q-switched laser are shown. It can be seen that despite the increase of the pump temperature, the peak power was still decreasing when the drive current was increased, but the lasing threshold was lowered from about 14 W to 9 W of incident pump power. To avoid further damage to the Cr:YAG crystal, the maximum incident pump power was chosen to be 13 W. It turned out that further increasing the incident pump power would not have increased the amount of UV light (Sec. 6.4).

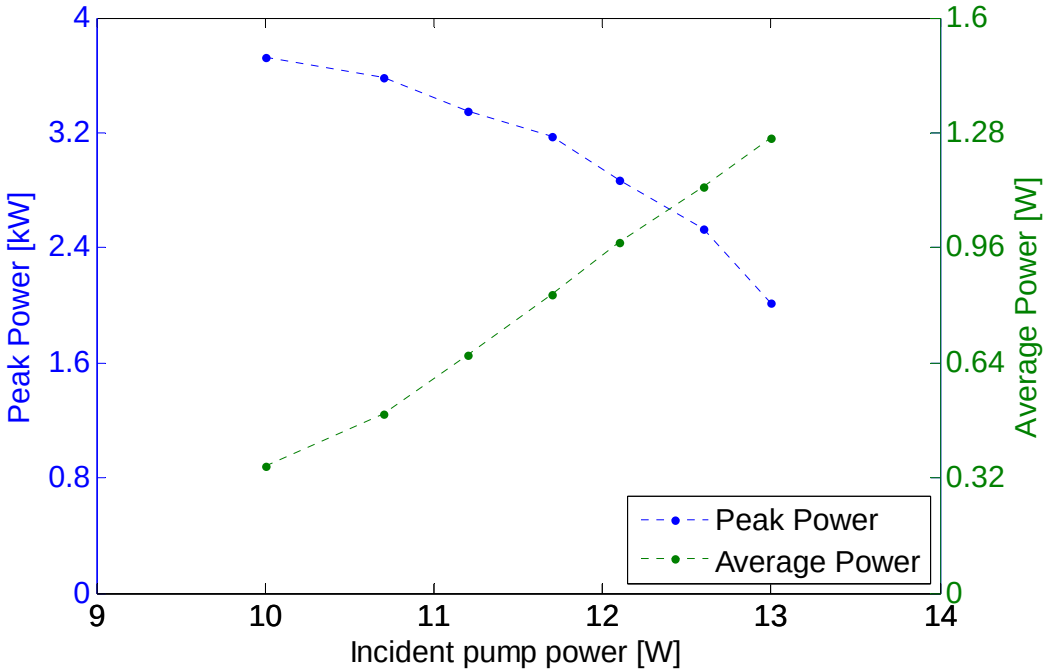

Figure 6.5: *Pulse peak power and average output power vs. pump laser drive current.*

The pulse width and repetition frequency are shown in Fig. 6.6, measured with a fast photo diode and an oscilloscope of 1 GHz bandwidth. The pulse width was measured in an average of 3 recorded pulses. The error bars show the standard deviation of the repetition frequency. As one can see, both the repetition frequency (4 kHz to 21 kHz) and the pulse width (16 ns to 20 ns) increased as the incident pump power was increased from 10 W to 13 W.

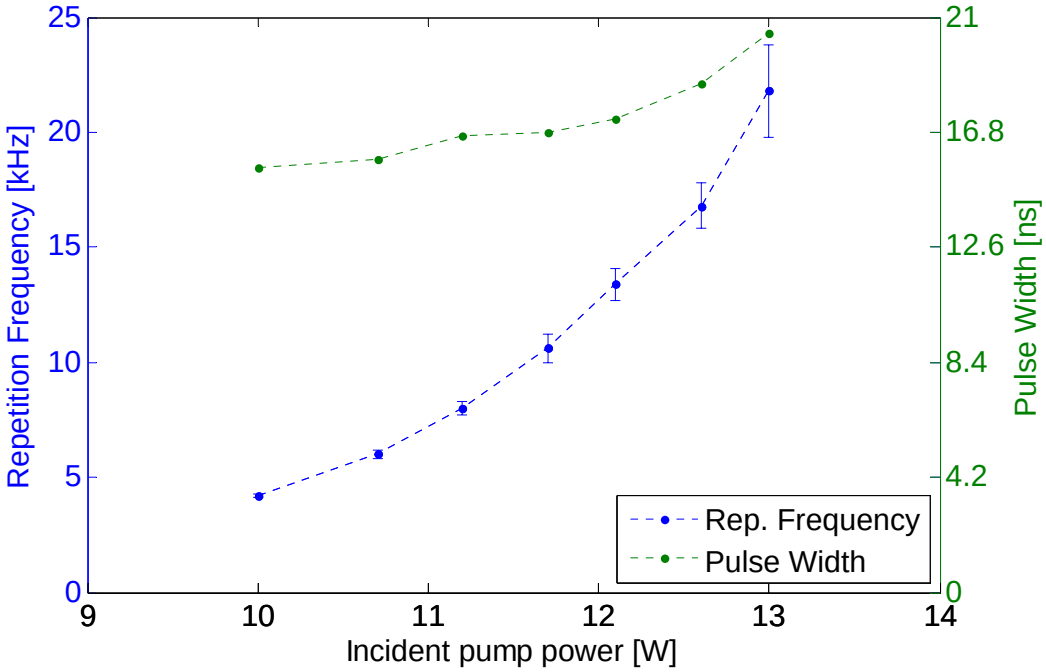

Figure 6.6: *Pulse width and repetition frequency vs. pump-laser drive current. The error bars show the standard deviation.*

A spectrum analyzer (ANDO-6315A) with a resolution bandwidth of 0.05 nm was used to analyze the spectrum. The results are given in Fig 6.7 recorded at 10 W and 13 W of incident pump power, respectively. As can be seen the spectral power distribution is slightly redshifted when the incident pump power is increased from 10 W to 13 W. The bandwidth is about 0.16 nm and 0.23 nm for the spectra at 10 W and 13 W of incident pump power, respectively. The presence of multiple peaks in the spectra indicates that oscillation on several longitudinal modes occurred with a frequency separation between adjacent modes about 24 GHz. The mode separation corresponds to the optical length of the Yb crystal, which indicates that the crystal was acting as a Febry-Pérot etalon, limiting the allowed modes in the cavity.

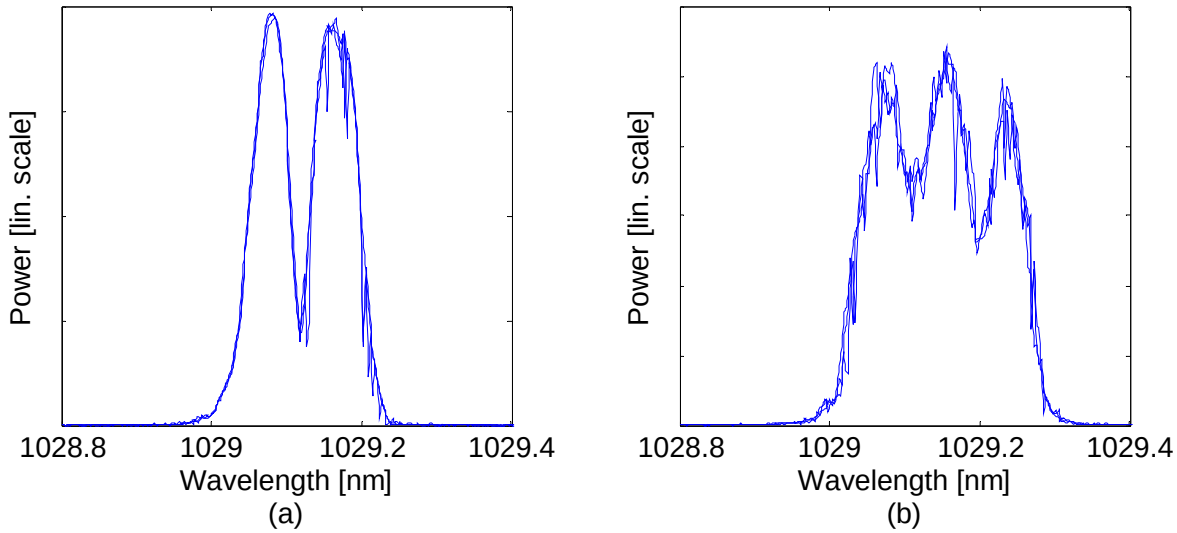

Figure 6.7: *Spectra of the pulsed Yb:KYW laser. The spectra in (a) and (b) were recorded at 10 W and 13 W incident pump power, respectively. In each image, spectra from three recordings are plotted on top of each other.*

The beam quality factor M^2 of the laser beam was measured at 12 W of incident pump power to be about 1 for both the direction of the polarization and the perpendicular direction by using the knife-edge technique described in Sec. 2.1. The beam at 12 W of incident pump power was chosen to represent a typical beam from the laser. According to simulations based upon the data from the measurement, the mode $1/e^2$ radius inside the cavity just before the output coupler was about 180 µm. When simulating the cavity, the same radius becomes about 150 µm. This indicates that thermal lensing occurs in the system. It is, however, difficult to distinguish if the thermal lensing occurs it the Yb:KYW, in the Cr:YAG or in both of them.

To get an idea about how much the Yb crystal absorbed the pump, an absorption measurement was conducted in the same way as described in Sec. 4.1. The measurement was conducted when the laser was lasing in cw without the Cr:YAG, because it would be difficult to distinguish the pump absorbed by the Yb:KYW from pump absorbed by the Cr:YAG when the laser was lasing in Q-switched mode. In Fig. 6.8 the result from the measurement is shown. As one can see, the absorption was higher when lasing occurred. This was expected and is discussed in Sec. 4.1. The curve showing the absorption when no lasing occurred has the highest value at 35 A of drive current. The peak of the absorption curve was expected to occur at a drive current lower than the maximum, since the temperature of the pump laser had been adjusted as described above. The absorption of pulsed laser should be in between the two curves. As the repetition frequency increases, the absorption of the pulsed system should approach the absorption of the cw lasing system. Note that for the pulsed laser, a maximum pump power of 13 W was used.

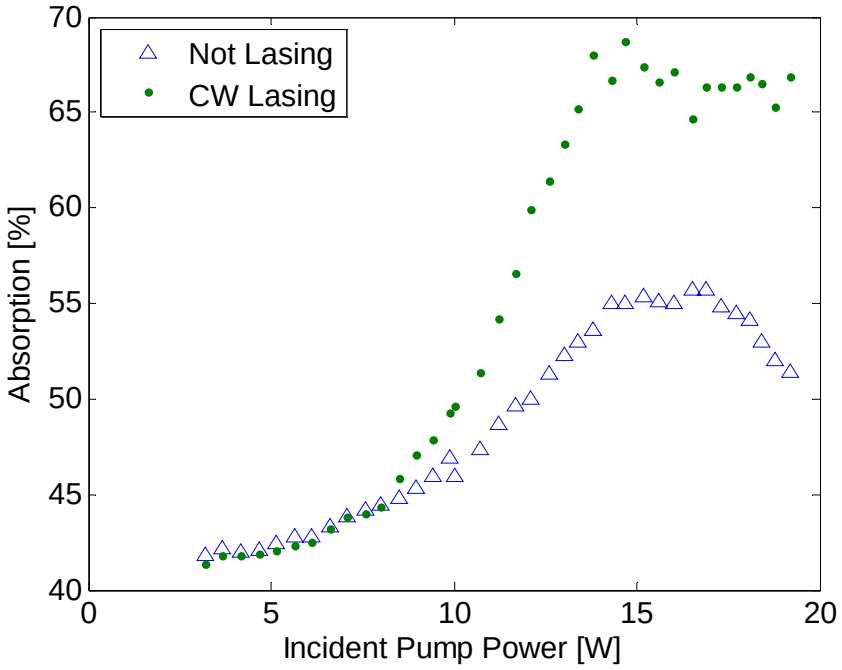

Figure 6.8: *Absorption vs. pump laser drive current, with and without laser action. The green markers (at lasing) show the absorption both above and below threshold.*

6.3 Second harmonic generation to green

In this chapter generation of green light at a wavelength of 515 nm is described using the Q-switched laser.

The beam from the pulsed laser was collimated by a lens with focal length of 100 mm placed 7.3 cm after the output coupler. The second harmonic was generated in a 10 mm long LBO crystal cut for type I phase matching at $\theta = 90^{o}$ and $\Phi = 13.6^{o}$. The nonlinear coefficient, d_{eff}, was 0.83 pm/V at 300 K and the Poynting vector walk-off was 8.16 mrad for the second harmonic wave, [19].

Five lenses with different focal length were tried to focus the fundamental beam into the LBO crystal. The beam propagation was simulated to estimate the size of the beam waist for each lens, based on the measurement of the fundamental beam size. In Fig. 6.9 the measured average output power of green is shown for different focusing conditions and pump powers. The highest average green power was with a 30 μm beam waist acquired from the lens with a focal length of 50 mm. This is the system that was used for further experiments. According to Boyd-Kleinman theory, see [20] and references therein, the optimal beam waist should be about 24 μm. The maximum average power of green was about 130 mW with the conversion efficiency, with respect to the fundamental wave, of about 10 %. Note that the highest conversion efficiency was about 13 % and occurred at 10 W of incident pump power. This is due to the decrease in peak power as described in the previous section.

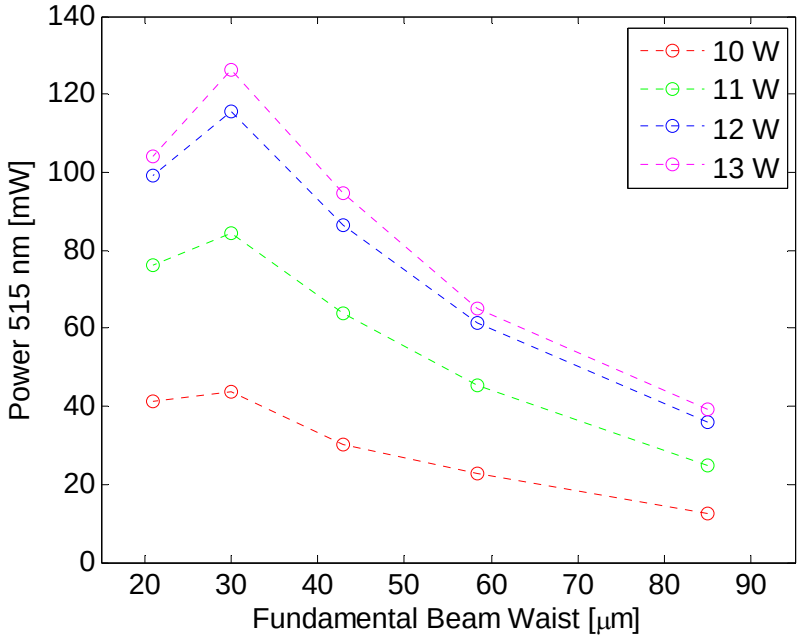

Figure 6.9: *Power of the second harmonic vs. fundamental beam waists for different pump laser drive currents.*

In Fig. 6.10, the average power of green is shown versus the incident pump power for the system with a fundamental beam waist of 30 μm.

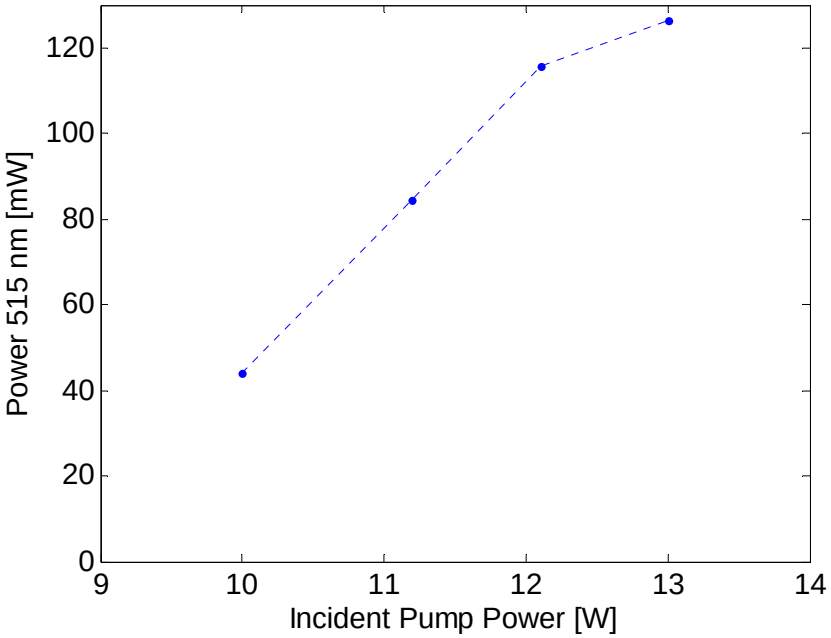

Figure 6.10: *Average power of green vs. incident pump power.*

The generated second harmonic beam had an elliptic shape. The beam quality factor, M^2, was measured at 10 W of incident pump power by using the knife-edge technique (Sec. 2.1) to be about 1 in both the direction. It was assumed that the beam quality was lowest at 10 W of

incident pump power, since the peak power was the highest, which lead to highest conversion efficiency and thus the largest influence of Poynting-vector walk-off. The data from the measurement were used to simulate the propagation of the beam. According to the simulation, the beam waist $1/e^2$ radii were 37 μm and 46 μm along the short and long axis, respectively, at the end surface of the LBO. The long axis was in the direction of the Poynting-vector walk-off. This corresponds to what could be observed with the naked eye.

A spectrum analyzer (ANDO-6315A) with a resolution bandwidth of 0.05 nm was used to analyze the spectrum. The results are given in Fig 6.11 at 10 W and 13 W of incident pump power, respectively. As can be seen the spectral power distribution is slightly red shifted when the incident pump power is increased from 10 W to 13W. The bandwidth is approximately 0.09 nm and 0.12 nm for the spectra at 10 W and 13 W of incident pump power, respectively. The bandwidth of the two spectra corresponds to half the bandwidth of the two spectra of the fundamental wave (Fig. 6.7), as expected.

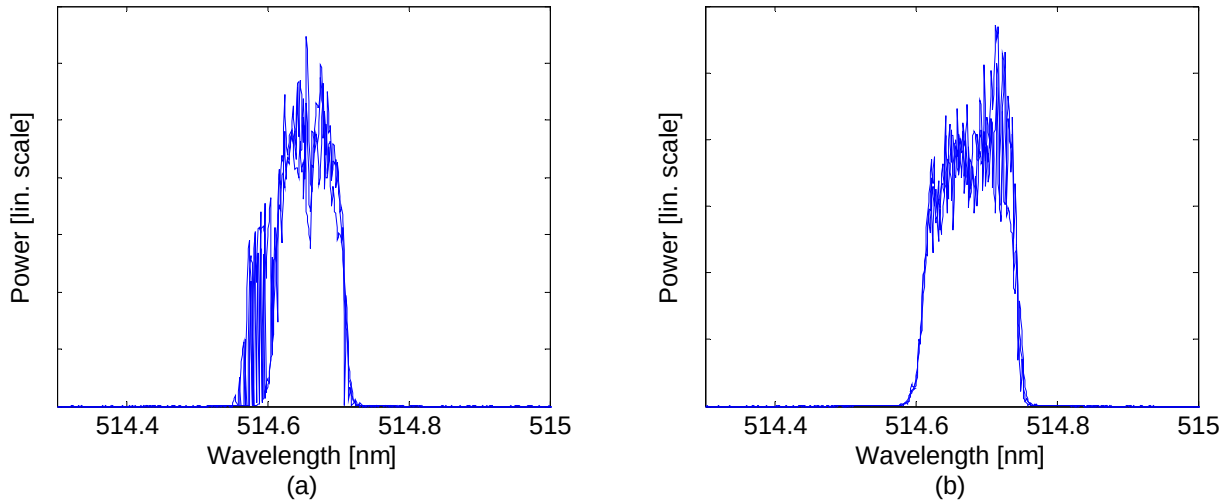

Figure 6.11: *Spectra of the pulsed Yb:KYW laser. The spectra in (a) and (b) were recorded at 10 W and 13 W incident pump power respectively. In each image, spectra from three recordings are plotted on top of each other.*

6.4 Sum frequency generation to UV

The goal with the experiments described in this section was to generate UV-light by mixing the second harmonic and the fundamental beams through sum frequency generation (SFG).

UV light at a wavelength of about 343 nm was generated in a 10 mm long LBO crystal. The crystal was cut for type II phase matching at $\theta = 50.5^{o}$ and $\Phi = 90^{o}$. The nonlinear coefficient, d_{eff}, was 0.46 pm/V at 300 K and the Poynting vector walk-off was 9.24 mrad for the second harmonic wave, [19].

A schematic drawing of the setup is shown in Fig. 6.12. Fig. 6.13 shows a picture of the setup. The green light is the second harmonic and the violet is fluorescence from a piece of paper exposed to the UV beam. Both the fundamental beam (Sec. 6.2) and the green second harmonic beam (Sec. 6.3) were collimated by the same lens with 30 mm focal length and broadband AR coating for the visible region and losses for the fundamental of about 15 %. Two lenses with the focal length of 40 mm and 50 mm were tried separately to focus the beams into the LBO used for SFG. The 40 mm lens had broadband AR coating for the visible region and 50 mm lens has broadband AR coating for both the regions around 1064 nm and 532 nm.

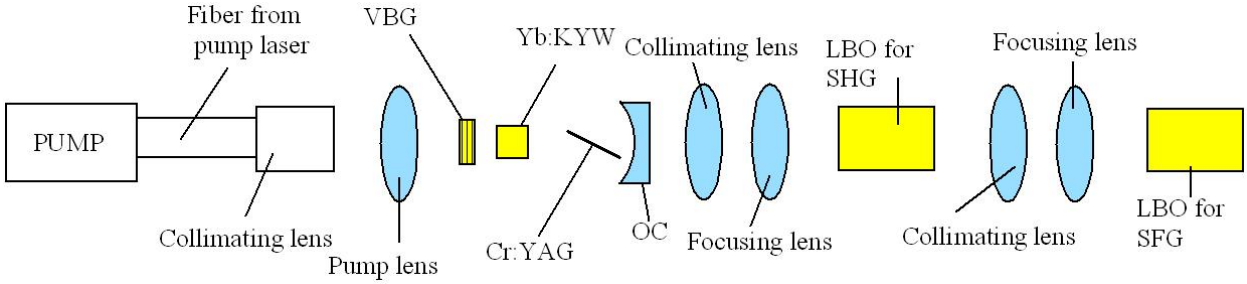

Figure 6.12: *Schematic drawing of the setup.*

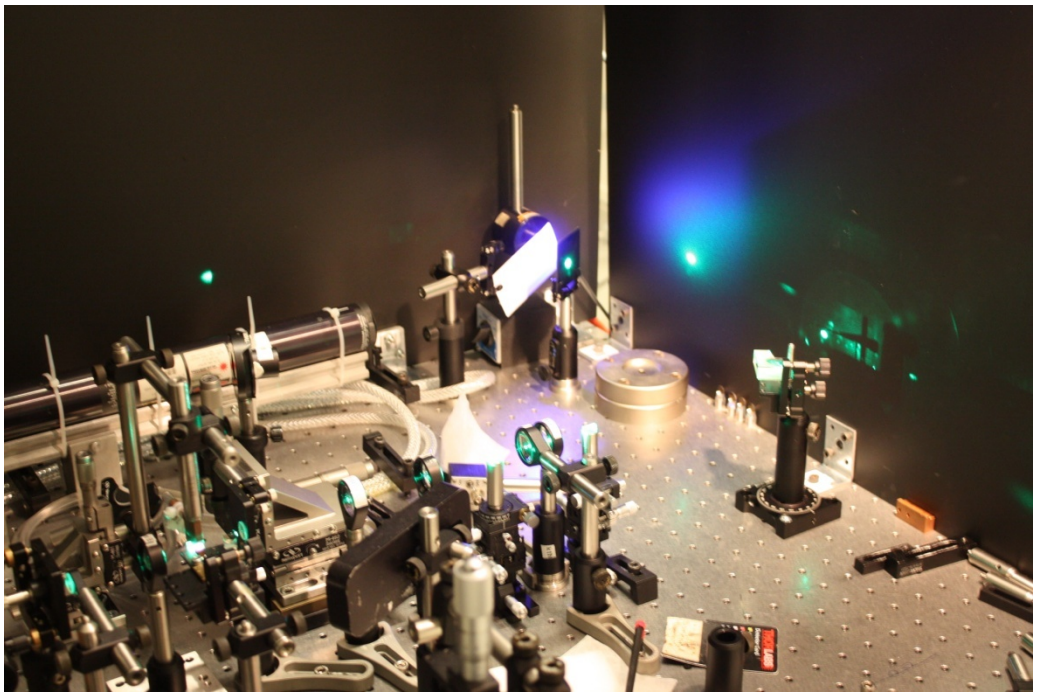

Figure 6.13: *Photography of the experimental setup.*

The propagation of the green beam was simulated to estimate its size inside the LBO crystal. The beam waist $1/e^2$ radii were about 30 µm and 60 µm along the short and long axis, respectively, when the beam was focused by the 40 mm lens. The 50 mm lens provided the beam waist about 40 µm and 80 µm along the short and long axis, respectively. The position of the focus for the

long and short axis did not coincide along the propagation direction. The difference in beam size in the direction of the long axis was, however, only a few micro-meters.

In Fig. 6.14 the measured average power of UV light for different pump currents and focusing is shown. The highest average power of around 22 mW was found for the system constructed with the 40 mm lens at 12 W incident pump power.

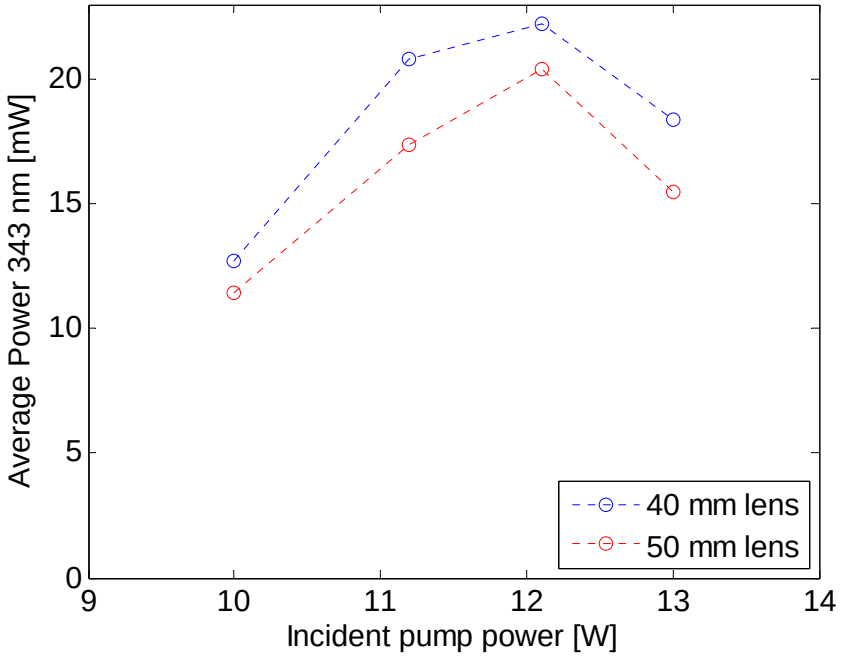

Figure 6.14: *Average power of UV vs. incident pump power.*

In Fig. 6.15 the conversion efficiency with respect to the green pump is shown. The green pump was chosen since it was assumed that it limited the process of SHG to a larger extent than fundamental beam. The maximum conversion efficiency was around 29 % at 10 W incident pump power for the system with the 40 mm lens.

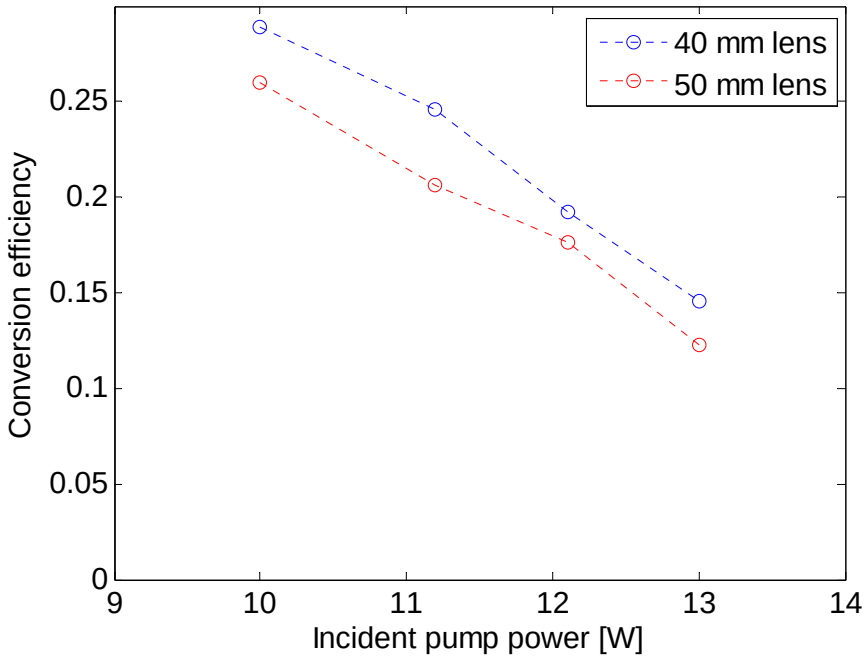

Figure 6.15: *Conversion efficiency with respect to the green pump. The legend shows the size of the beam waist according to simulations.*

In the measurements for both the 40 mm lens and the 50 mm lens, the conversion efficiency decreases with increasing pump laser power. Also, the average power of UV decreased when the incident pump power was increased from 12 W to 13 W. Due to the cubic dependence of the UV electric field on the fundamental electric field, both these effects are considered to be caused by the observed decrease in peak power in the fundamental beam with increasing pump laser power (Sec. 6.2).

The generated UV-beam had an elliptic shape, and the beam quality factor, M^2, was measured to be about 1 in both directions, for the system built with the 40 mm lens at 10 W incident pump power, using the knife-edge technique (Sec. 2.1). The choice of pump laser power was based upon the assumption that the beam quality would be lowest at the highest conversion efficiency.

In Fig. 6.16 the optical efficiency referring to ratio between the average UV power and the pump laser output power is shown. As one can see the maximum optical efficiency was about 0.16 % at 11 W incident pump power with the 40 mm lens system.

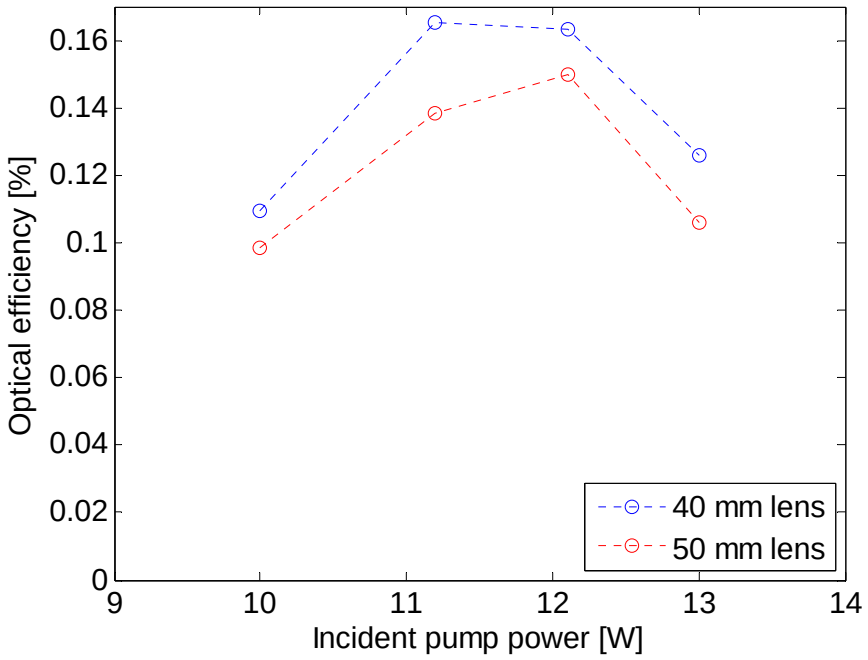

Figure 6.16: *Optical efficiency with respect to pump output power vs. incident pump power.*

6.5 Damage to components

In this section the damage to the components during the Q-switching experiments is presented.

To investigate whether any of the components of the laser had been damaged during the experiments, they were examined in a microscope. Disregarding the cracked Cr:YAG crystal discussed in Sec. 6.2, the only component that showed clear signs of damage was the Yb:KYW crystal. As shown in Fig. 6.17, there were burn marks in both the actual crystal and its coating.

During the experiments with the pulsed laser, it occurred that the laser stopped lasing. Also, in the experiments to optimize the initial transmission of the Cr:YAG (Sec. 6.2), when using Cr:YAG crystals of initial transmission of 90 % and 86 % lasing was only achieved for a few pulses. In both these cases, the position of the laser mode inside the Yb crystal needed to be changed for the laser to start lasing again. It is likely that the burn marks come from these occasions.

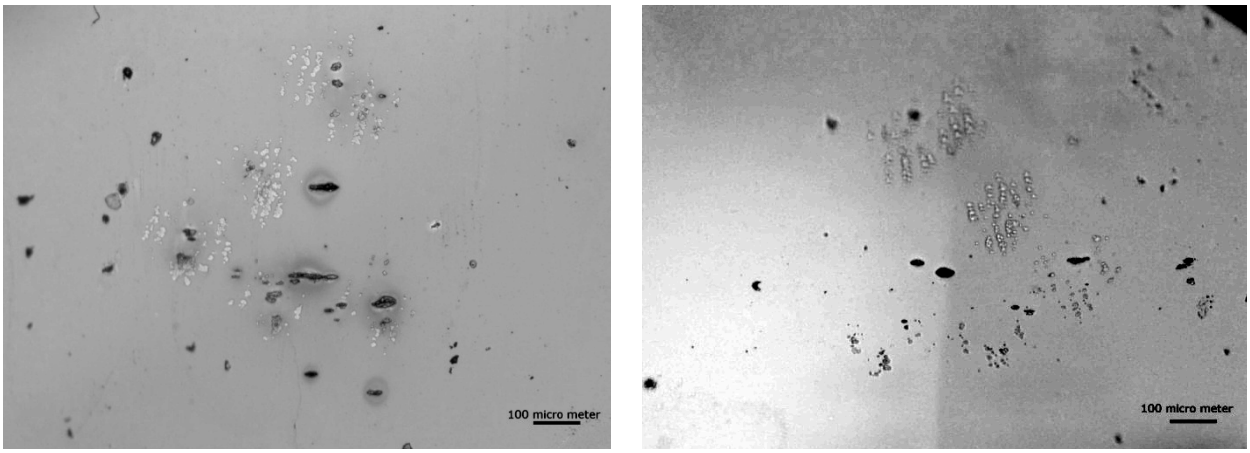

(a) (b)

Figure 6.17: *Pictures showing the surface of the Yb:KYW. In (a) and (b) the surface towards the pump and the surface towards the Cr:YAG is shown, respectively.*

6.6 Discussion

Discussion and conclusions

A diode-pumped Yb:KYW laser has been constructed, using a volume Bragg grating as input coupler. The spectrum of the laser was successfully locked at 1029 nm with a bandwidth of 0.23 nm at FWHM. When operating in c-w mode, the laser generated 5.1 W at an incident pump power of 19 W.

A linear cavity pulsed laser was built using Cr:YAG as a saturable absorber. The highest average output power was 1.3 W at 13 W of incident pump power. The highest peak power was 3.8 kW at 10 W of incident pump power with a pulse duration time of 16 ns at FWHM. As the incident peak power increased from 10 W to 13 W, the peak power decreased from 3.8 kW to 2 kW, the repetition rate increased from 4 kHz to 20 kHz and the pulse width increase from 16 ns to 21 ns. It is believed that the phenomena of decreasing peak power is due to the pump bleaching the Cr:YAG in addition to the laser itself. The experiments show that damage to components is a limiting factor that needs to be taken in to account when the laser is to be optimized.

For comparison, *Liu et al.* [13] constructed a similar linear cavity laser with a Cr:YAG as a saturable absorber, also placed in there cavity after the gain medium, Yb:KLuW. It should be noted that they had not taken any measure for spectral control. The average power they obtained was about the same for the same incident pump power. However, their laser could be pumped by incident pump power up to 24 W, without the problems that limited the incident pump power in our experiments. Also, different from our results. *Liu et al.* reported to have obtained pulse profiles that "*remained nearly unchanged, independent of the power level*". Furthermore, they achieved peak power of 77 kW with a pulse width of 2.2 ns at FWHM. Considering the result presented in [13], it is concluded that our laser could be optimized to obtain higher peak power.

The pulsed laser was successfully used to generate green light through the process of second harmonic generation (SHG) in a 10 mm long LBO crystal. The achieved wavelength was around 514.7 nm, which is an Argon laser line. This means that Argon lasers can be replaced by a frequency doubled Yb:KYW laser, engineered with a volume Bragg grating for spectral control. At an incident pump power of 13 W, 130 mW of green was achieved with an optical efficiency of 10 % with respect to the fundamental beam. It is considered that higher peak power would increase the conversion efficiency. Also, since LBO has a low effective nonlinear coefficient (0.83 pm/V) using a crystal with a higher nonlinear coefficient without walk-off, such as PPKTP should result in higher conversion.

The goal to generate UV at a wavelength of about 343 nm was achieved through the process of sum frequency generation (SFG) in a 10 mm long LBO. The maximum average output power was about 22 mW and the optical efficiency with respect to green was about 20 %. However, the decreasing peak power of the pulsed laser caused the optical efficiency to decrease as the pump power increased. Another effect of the decreasing peak power was that the average power of UV peaked at an incident pump power of 12 W, i. e. not at the maximum pump power. The overall optical efficiency of the system, referring to the ratio between the average UV power to pump laser power, was around 0.16 %. This is expected to increase if PPKTP is used for the second harmonic generation. The achieved wavelength of 343 nm is in between the laser lines of a Nitrogen laser (337 nm) and an Argon laser (351 nm). This means that after optimization this laser would be a good candidate for replacing these two gas lasers.

Future work

A folded cavity should be designed to avoid bleaching the Cr:YAG with the pump. The cavity should also be optimized with respect to peak power and the limiting damage threshold of the components. The optimization should be conducted in such a way that the maximum pump power could be used without breaking the Yb:KYW or the Cr:YAG. Also, PPKTP should be used for the process of second harmonic generation. The generated green beam should thereafter be used together with the fundamental beam to generate the third harmonic through sum frequency generation in a nonlinear crystal cut for type I birefringent phase matching. Also, the option of using quasi phase matching in Lithium tantalate for the SFG process should be investigated.

7 References

1. **W.T. Silfvast,** *Laser Fundamentals.* USA : Cambridge University Press (1996).

2. **B. Jacobsson, J. E. Hellström, V. Pasiskevicius and F. Laurell,** *Widely tunable Yb:KYW laser with a volume Bragg grating*, Opt. Express **15**, 1003-1010 (2007).

3. **N. V. Kuleshov, A. A. Lagatsky, A. V. Podlipensky, V. P. Mikhailov, G. Huber.** *Pulsed laser operation of Yb-doped $KY(WO_4)_2$ and $KGd(WO_4)_2$.* Opt. Lett. **22**, 1317-1319 (1997) .

4. **B. Jacobsson,** *Experimental and theoretical investigation of a volume-Bragg-grating-locked Yb:KYW laser at selected wavelengths*, Opt. Express **16**, 6443-6454 (2008).

5. **O. Svelto,** *Principles of Lasers, 4th ed.* Milan : Springer (1998).

6. **A. E. Siegman,** *Lasers.* Mill Valley, California : University Science Books (1986).

7. **Eksma optics.** [Online] http://www.eksmaoptics.com/en/p/passive-q-switches-500.

8. **W. Koechner,** *Solid-State Laser Engineering, 6th ed.* USA : Springer (2006).

9. **H. Ridderbusch and T. Graf,** *Saturation of 1047- and 1064-nm Absorption in Cr^{4+}:YAG Crystals*, IEEE J. Quantum Electron. **43**, 168-173 (2007).

10. **A. S. Grabtchikov, A. N. Kuzmin, V. A. Lisinetskii, V. A. Orlovich, A. A. Demidovich, M. B. Danailov, H. J. Eichler, A. Bednarkiewicz, W. Strek and A. N. Titov.** *Laser operation and Raman self-frequency conversion in Yb:KYW microchip laser,* Appl. Phys. B **75**, 6-7 (2002).

11. **A. A. Lagatsky, A. Abdolvand and N. V. Kuleshov.** *Passive Q switching and self-frequency Raman conversion in a diode-pumped $Yb:KGd(WO_4)_2$ laser*, Opt. Lett. **25**, 616-618 (2000) .

12. **J. Liu, U. Griebner, V. Petrov, H. Zhang, J. Zhang and J. Wang,** *Efficient continuous-wave and Q-switched operation of a diode-pumped $Yb:KLu(WO_4)_2$ laser with self-Raman conversion*, Opt. Lett. **30**, 2427-2429 (2005) .

13. **J. Liu, V. Petrov, H. Zhang and J. Wang.** *Power scaling of a continuous-wave and passively Q-switched $Yb:KLu(WO_4)_2$ laser end-pumped by a high-power diode*. Appl. Phys. B **88**, 527−530 (2007).

14. **R. W. Boyd,** *Nonlinear Optics 3ed.* New York : Academic press, 2008.

15. **Newlight Photonics.** [Online] http://www.newlightphotonics.com/lbo-properties.html.

16. **K. Seger and N. Meiser.** Measurements conducted at the Laser physics research group, Royal institute of technology (KTH).

17. **B. Jacobsson,** *"Spectral control of lasers and optical parametric oscillators with volume Bragg gratings",* PhD thesis, Royal Institute of Technology (KTH), Applied Physics (2008).

18. **P. Jelger, P. Wang, J. K. Sahu, F. Laurell and W. A. Clarkson,** *High-power linearly-polarized operation of a cladding-pumped Yb fibre laser using a volume Bragg grating for wavelength selection*, Opt. Express **16**, 9507-9512 (2008).

19. **Software package - SNLO,** http://www.as-photonics.com/SNLO.html.

20. **Y. F. Chen, Y. C. Chen,** *Analytical functions for the optimization of second-harmonic generation and parametric generation by focused Gaussian beams*, Appl. Phys. B **76**, 645–647 (2003).